SEARCH FOR SEMILEPTONIC DECAYS OF PHOTOPRODUCED CHARMED MESONS

BY

RICHARD NEAL COLEMAN

A.B. University of California, 1972
M.S. University of Illinois, 1974

THESIS

Submitted in partial fulfillment of the requirements
for the degree of Doctor of Philosophy in Physics
in the Graduate College of the
University of Illinois at Urbana-Champaign, 1977

Urbana, Illinois

DISCLAIMER

SEARCH FOR SEMILEPTONIC DECAYS OF PHOTOPRODUCED CHARMED MESONS

BY

RICHARD NEAL COLEMAN

A.B. University of California, 1972
M.S. University of Illinois, 1974

THESIS

Submitted in partial fulfillment of the requirements
for the degree of Doctor of Philosophy in Physics
in the Graduate College of the
University of Illinois at Urbana-Champaign, 1977

Urbana, Illinois

SEARCH FOR SEMILEPTONIC DECAYS OF PHOTOPRODUCED CHARMED MESONS

Richard Neal Coleman, Ph.D.

Department of Physics

University of Illinois at Urbana-Champaign, 1977

In the broad band neutral beam at Fermilab, a search for photoproduction of charmed D mesons has been done using photons of 100 to 300 GeV. The reaction considered was

$$\gamma + \mathrm{Be} \rightarrow D\bar{D} + X \quad \begin{cases} \hookrightarrow \text{leptons} + \ldots \\ \hookrightarrow K^0_S n\pi^{\pm} \end{cases}$$

No statistically significant evidence for D production is observed based on the $K^0_S n\pi^{\pm}$ mass spectrum. The sensitivity of the search is commensurate with theoretical estimates of $\sigma(\gamma p \rightarrow D\bar{D} + X) \sim 500$ nb, however this is dependent on branching ratios and photoproduction models. An appendix contains data on a similar search for semileptonic decays of charmed baryons.

Acknowledgements

I am particularly grateful to my advisor Professor A. Wattenberg for his continued guidance, encouragement, and patience throughout my graduate study.

I would also like to thank the members of the experimental group for their dedication in performing the experiment and for many valuable discussions. They are: P. Avery, M. Binkley, J. Bronstein, J. Butler, L. Cormell, I. Gaines, G. Gladding, M. Goodman, M. Gormley, B. Knapp, J. Knauer, W. Lee, P. Leung, R. Messner, D. Nease, T. O'Halloran, R. Orr, J. Peoples, L. Read, J. Russell, J. Sarracino, S. Smith, D. Wheeler, A. Wijangco, D. Yount.

In addition I would like to acknowledge the technical support and hard work of K. Gray, L. Seward, S. Marino, and the Fermilab Proton Lab.

Special thanks go to my wife Jackie for her patience and understanding, in addition to the excellent job done in the typing and general preparation of this thesis.

This research was supported in part by the U.S. Energy Research and Development Administration under contract E(11-1)-1195.

Table of Contents

I. Introduction

As early as 1962-1964, several authors suggested the addition of a fourth quark to achieve a lepton-quark symmetry.[1] The fourth quark carries a new quantum number called charm which is violated in the weak interactions. In 1970 Glashow, Iliopoulos, and Maini showed that the charmed quark not only provides an elegant theory with four quarks and four leptons with identical weak couplings, but also explained the suppression of strangeness changing neutral currents.[2] The charm model predicts the existence of many charmed particles.[3] Since these particles had not been observed, it was speculated that the charmed quark was heavier than the other three. This assumption put the masses of the charmed particles in a relatively unexplored mass region.

In late 1974, two groups announced the discovery of a narrow resonance (J/ψ) with a mass of 3.1 GeV/c^2. At BNL[4] it was observed in the production of e^+e^- from proton-beryllium collisions. At SPEAR[5] it was seen in the production of hadrons from e^+e^- annihilation. Since the initial discovery of the J/ψ, its properties have been studied in great detail in e^+e^- annihilation.[6] It is an excellent candidate for a charm-anticharm quark ($c\bar{c}$) state with $J^{PC} = 1^{--}$. In addition another narrow state (ψ') has been observed at 3.7 GeV and is interpreted as an excited state of the $c\bar{c}$ state.[7] The extremely narrow widths of the J/ψ and ψ' are qualitatively explained using Zweig's rule.[8]

If the J/ψ and ψ' are $c\bar{c}$ states then a whole family of $c\bar{c}$ states should exist. These states will have parity $P = -(-1)^L$

and charge conjugation $C = (-1)^{L+S}$, where L is the orbital angular momentum and S is the spin of the $c\bar{c}$ state. The lowest mass states should have L = 0. The L = 1 states should be several hundred MeV higher. Therefore one expects a pseudoscalar ($J^{PC} = 0^{-+}$) partner of the J/ψ with mass near the mass of the J/ψ, as well as, three L = 1 states with slightly higher mass with $J^{PC} = 0^{++}$, 1^{++}, 2^{++}. At DORIS[9] a state at 2.85 GeV/c^2 has been observed which is generally interpreted as the pseudoscalar partner $J^{PC} = 0^{-+}$ of the J/ψ. Several groups[6] have reported four even charge conjugation states with masses between the J/ψ and ψ' mass. The properties of the radiative and hadronic decays measured so far suggest that these states correspond to the $J^{PC} = 0^{++}$, 1^{++}, 2^{++} partners of the J/ψ and the pseudoscalar partner ($J^{PC} = 0^{-+}$) of the ψ'.[10] There are quantitative difficulties with the predictions of the simplest charm models and the measured radiative and hadronic decay widths, and mass splittings. These problems and alternate interpretations are discussed in the literature.[11]

In addition to the $c\bar{c}$ states, there must be $c\bar{q}$ (or $\bar{c}q$) states where q refers to one of the three non-charmed quarks. It is important to note that any model introducing a fourth quark (c) will produce a variety of $c\bar{c}$ and $c\bar{q}$ states. However, the charmed quark as introduced by GIM to suppress strangeness changing neutral currents in a Weinberg-Salam[12] type theory has important implications for the decays of $c\bar{q}$ states. The weak interactions may mix the c quark with its isodoublet partner usually called $s' = -d \sin\theta_C + s \cos\theta_C$ where θ_C is the Cabibbo angle. This leads to selection rules, $\frac{\Gamma(\Delta C = \Delta S = 1)}{\Gamma(\Delta C = 1,\ \Delta S = 0)} \simeq \cot^2\theta_C \simeq 20$, where

C = charm, S = strangeness, and Γ = decay rate. The decay of a c quark to u quark is suppressed. The lowest mass $J^{PC} = 0^{-+}$ mesons formed from $c\bar{q}$ and $\bar{c}q$ states with C = ± 1 are:

$D^+ = c\bar{d}$	$D^0 = c\bar{u}$	$F^+ = c\bar{s}$
$D^- = \bar{c}d$	$\bar{D}^0 = \bar{c}u$	$F^- = \bar{c}s$

A few representative hadronic decays are listed below:

Cabibbo Angle Dependence	D^0	D^+
$\cos^4\theta_C$	$K^-\pi^+$, $\bar{K}^0\pi^+\pi^-$	$K^-\pi^+\pi^+$, $\bar{K}^0\pi^+$
$\cos^2\theta_C \sin^2\theta_C$	$\pi^-\pi^+$	$\pi^-\pi^+\pi^+$
$\sin^4\theta_C$	$K^+\pi^-$, $K^0\pi^+\pi^-$	$K^+\pi^+\pi^-$, $K^0\pi^+$

For leptonic decays, the model predicts that $D^0 \to K^-\ell^+\nu$ (not $K^+\ell^-\nu$) and $D^+ \to \bar{K}^0\ell^+\nu$ (not $K^0\ell^+\nu$) are enhanced by $\cot^2\theta_C$ over the decays $D^0 \to \pi^-\ell^+\nu$ and $D^+ \to \pi^0\ell^+\nu$. Thus $c\bar{q}$ states in the GIM charm model should decay weakly (narrow widths) with selection rules that imply exotic decays and correlations between kaons and leptons. Exotic decays are those in which the electric charge of the hadrons is opposite to the strangeness. Based on the J/ψ and ψ' masses, De Rújula, Georgi, and Glashow predicted the masses of the D mesons to be 1.83 ± 0.03 GeV and the lowest mass charmed baryon (Λ_c) to be 2.25 ± 0.05 GeV.[13]

In the summer of 1976 evidence was found for several $c\bar{q}$ states with the properties corresponding to the charmed mesons (D^0, D^+) and a charmed baryon (Λ_c).[14,15,16] At SPEAR in e^+e^- annihilation narrow peaks were found in $K^{\mp}\pi^{\pm}$ and $K^{\mp}\pi^{\pm}\pi^{\mp}\pi^{\pm}$ mass spectra for data taken at center-of-mass energies (E_{cm}) 3.9 and 4.6 GeV.[14] The mass was found to be 1865 ± 15 MeV and its width less than the resolution of 40 MeV. This narrow resonance is a strong

candidate for the D^0 meson. Another narrow peak was found in the $K^{\pm}\pi^{\mp}\pi^{\mp}$ mass spectrum for data at E_{cm} = 4.03 GeV.[15] There was no corresponding peak in the mass spectra of the non-exotic combination of $K\pi\pi$. Its mass was found to be 1876 ± 15 MeV and its width less than the resolution. This state is a strong candidate for the D^- meson. The SPEAR[17] group also sees an enhancement in the $K^0_S 2\pi$ mass spectrum at the D^0 mass. There are also indications of the photoproduction of D^0 followed by its decay into $K_S 4\pi$.[18]

Both the $D^{\pm}$ and D^0 are produced in association with systems of comparable or higher mass (D or D*). The mass of the recoil system associated with D^0 production at E_{cm} = 4.03 GeV has been studied at SPEAR[17] in e^+e^- annihilation. The D* is the $J^P = 1^-$ cu or cd state which should decay either strongly (pion emission) or electromagnetically (photon emission) to a D meson.[19,20] Recent results[21] indicate that kinetic energy in the decay $D^{*0} \to D^0\pi^0$ is about 3 MeV and the D^{*0} mass is 2005. The dominant D^{*0} decays are $D^{*0} \to D^0\pi^0$ and $D^{*0} \to D^0\gamma$ whose decay rates are approximately equal (1.0 ± 0.3). The D^0 mass is determined to be 1868 ± 2 MeV. Finally and with less certainty the $D^{*+} \to D^0\pi^+$ decay does not overwhelmingly dominate the $D^{*+} \to D^+\gamma$ and $D^{*+} \to D^+\pi^0$ decay modes.[11] Recently the charged D* has been observed directly from the decays where $D^{*+} \to D^0\pi^+$ and then $D^0 \to K^-\pi^+$.[22]

In a simple model of D production, one pictures the $c\bar{c}$ pair to be created by the virtual photon in e^+e^- annihilation and the mesons are formed by combining with light quarks from the vacuum. This implies the ratio of $D\bar{D}$:$D^*\bar{D}$ + $D\bar{D}^*$:$D^*\bar{D}^*$ is 1:4:7.[19,20] Unfortunately these ratios are very sensitive to dynamical effects.[11,23]

However the qualitative prediction that D* production dominates D production is verified in e^+e^- annihilation.

Evidence exists for the semi-leptonic weak decays of charmed particles. Two groups at DORIS[24,25] observe hadrons and a single electron resulting from the decay of a particle with mass between 1.84 and 2.0 GeV. Anomalous single muon events have been seen in multiprong events at SPEAR.[26] The properties of the single lepton events will be discussed in more detail later. Evidence for weakly decaying hadrons is also found in neutrino interactions. Anomalous $e^{\pm}\mu^{\mp}$ events have been found in bubble chamber experiments at CERN and Fermilab.[27] Anomalous dimuon events have been observed in ν-counter experiments at Fermilab.[28]

Evidence for charmed baryons comes from a Brookhaven neutrino event[29] and a resonance in the $\bar{\Lambda}3\pi^-$ mass spectrum observed in our photoproduction experiment at Fermilab.[16] The Brookhaven experiment reported a charmed baryon candidate with a $\Lambda\pi^+\pi^+\pi^-$ mass of 2.244 GeV/c^2 and a higher mass $\Lambda\pi^+\pi^+\pi^-\pi^-$ combination at 2.426 GeV/c^2. The photoproduction experiment reported a peak in $\bar{\Lambda}3\pi^-$ at $2.26 \pm .01$ GeV/c^2 with a width of less than 75 MeV. No resonance was seen in the corresponding non-exotic channel. Evidence is also presented for higher mass states near 2.5 GeV which decay into the 2.26 GeV state. The 2.26 GeV state is a good candidate for the lowest mass charmed baryon (Λ_c or C_o^+ in reference 3), the charmed analogue of the Λ(1115 MeV). Charmed baryons may decay semileptonically, for example $\Lambda_c \to \Lambda\ell\nu$. (See Appendix B.)

This thesis reports on a search for the photoproduction of a pair of charmed D-mesons and the subsequent decay of one D into

leptons and the other D into $K^0_S\, n\pi^{\pm}$ ($n = 1, 2, 3, 4$). If the ψ is a $c\bar{c}$ state then Zweig's rule[8] suggests final states in the ψ-nucleon collision should contain charmed quarks. ψ production can be combined with vector dominance assumptions to give $\sigma^{elastic}(\psi N)/\sigma^{tot}(\psi N) \sim$ few percent.[30,31] Thus the majority of c quarks produced in ψ-nucleon collisions must come from states with $C = \pm 1$ rather than the ψ. This implies $\sigma^{tot}(\psi N) \simeq \sigma(\psi N \to X_c \bar{X}_c + \text{anything})$ where X_c is any $C = \pm 1$ state. Applying vector dominance principles gives $\sigma(\gamma N \to X_c \bar{X}_c + \text{anything}) \simeq 500 \times \lambda$ (nb) where λ is a parameter to describe corrections to the vector dominance model. $\lambda = 1$ implies complete vector dominance validity.[32] Sivers, Townsend, and West estimate $\sigma(\gamma p \to X_c \bar{X}_c + \ldots) \geq 300$ nb. $\sigma^{tot}(\psi N)$ can be determined without using vector dominance assumptions by measuring the A (nucleon number) dependence of ψ photoproduction. The result is $\lambda = 0.29$.[31] Chen, Kane, and Yao also use vector dominance arguments to predict $\sigma(\gamma p \to D\bar{D} + X) \gtrsim 500$ nb.[33] The charmed baryon (Λ_c) photoproduction cross-section though not accurately determined seems compatible with a few hundred nanobarn signal. However a measurement of inclusive muon production at $E_\gamma = 18$ GeV and $p_\perp^\mu = 1$ GeV, finds $\sigma(\gamma p \to D\bar{D} + X) \simeq 20$ nb if the branching ratio $B_{D \to \mu} = .10$.[31] Uncertainties in $B_{D \to \mu}$ and the experimental acceptance could be responsible for the small value of $\sigma(\gamma p \to D\bar{D} + X)$ obtained. So the cross-section for the photoproduction of a pair of charmed D-mesons in this experiment is in the range of 50 - 500 nb/nucleon.

The total semileptonic decay rate can be estimated by replacing the decay of a c quark to the decay $\mu \to e\bar{\nu}_e\nu_\mu$.[3] The

result is $\Gamma(D \to \ell\nu + \text{hadrons}) \simeq (\frac{m_c}{m_\mu})^5 \Gamma(\mu \to e\bar{\nu}_e\nu_\mu) \sim 3 \times 10^{11}$ sec^{-1} where $m_\mu(m_c)$ = muon (c-quark) mass. The decay $D^+ \to \bar{K}^0\ell^+\nu$ can be related to $K^0 \to \pi^-\ell^+\nu$ assuming approximately equal form factors to give

$$\Gamma(D^+ \to \bar{K}^0\ell^+\nu) \simeq (\frac{m_D}{m_K})^5 \left[f(x_D)/f(x_K)\right] \cot^2\theta_C \, \Gamma(K^0 \to \pi^-\ell^+\nu)$$

where

$$f(x) = 1 - 8x^2 + 8x^6 - x^8 - 24x^4 \ln x$$

$$x_D = \frac{m_K}{m_D} = \text{ratio of } \bar{K}^0 \text{ mass to } D^+ \text{ mass}$$

$$x_K = \frac{m_\pi}{m_K} = \text{ratio of } \pi^- \text{ mass to } K^0 \text{ mass}$$

Using $\Gamma(K^0 \to \pi^-e^+\nu) = \Gamma(K_L^0 \to \pi^-e^+\nu) \simeq 10^7$ sec^{-1} gives $\Gamma(D^+ \to \bar{K}^0\ell^+\nu) \simeq 10^{11}$ sec^{-1}.[3] The leptonic decay rates for a D meson can be estimated using the decay $K \to \mu\nu$. The result is $\Gamma(D^+ \to \mu^+\nu_\mu) \simeq (\frac{m_D}{m_K}) \Gamma(K^+ \to \mu^+\nu_\mu) \simeq 2 \times 10^8$ sec^{-1}, therefore $\Gamma(D \to \ell\nu)/\Gamma(D \to \ell\nu + \text{hadrons}) \simeq 10^{-2}$ to 10^{-3}. In the same spirit, one estimates:

$$\Gamma(\text{charm} \to \text{hadrons}) \simeq 3(\frac{m_c}{m_\mu})^5 \cos^2\theta_C \;\; \Gamma(\mu \to e\nu_e\nu_\mu)$$

$$\simeq 10^{12} \text{ sec}^{-1}$$

These rough estimates imply $B_\ell \simeq 10\%$. Dilepton events from neutrino interactions suggest $B_\ell \simeq 10\%$ for some weighted average over different charm particles produced.[28] Recently DASP[24] has observed final states with a single electron plus hadrons. From the threshold behavior they conclude the source's mass to be 1.8 to 2.0 GeV. Their results are $20\% \geq B_\ell(H \to eX) \geq 10\%$ where H is some average over charged and neutral D mesons. The PLUTO[25] group has found a correlation between electrons and K_S^0's with $\sigma(e^+e^- \to eK^0 + X) \simeq 3$ nb within systematic uncertainties of a factor of two. This can be

compared to the DASP[24] result $\sigma(e^+e^- \to e^\pm + \text{hadrons}) \simeq 1$ to 4 nb. The high track multiplicity and the soft electron momentum spectrum of the events favors a charm origin rather than heavy lepton. The electron momentum spectrum indicates a significant fraction of the decays are $D \to K^*(892\ \text{MeV})\ell\nu$. Estimates give $\frac{\Gamma(D \to K\ell\nu)}{\Gamma(D \to K^*\ell\nu)} \simeq 1$ and $\frac{\Gamma(D \to K\ell\nu) + \Gamma(D \to K^*\ell\nu)}{\Gamma_{\text{tot semileptonic}}} \simeq 80\%$[34,35,36] (which seems consistent with the data).

For the hadronic decay modes of the D-meson the statistical-isospin model[37,38] provides some useful estimates. In particular for $D \to K^0 n\pi^\pm$, the model predicts $\frac{\Gamma(D \to K^0 n\pi^\pm)}{\Gamma(\text{hadronic})} = .13, .12, .11,$ and .04 for n = 1, 2, 3, 4. The predictions of this model can be compared to the SPEAR results[17] at $E_{cm} = 4.03$ GeV which are

$$2B(D^0 \to K^-\pi^+)\ \sigma(D^0) = 0.52 \pm 0.05\ \text{nb}$$
$$2B(D^0 \to K^0\pi^+\pi^-)\ \sigma(D^0) = 0.80 \pm 0.21\ \text{nb}$$
$$2B(D^0 \to K^-2\pi^+\pi^-)\ \sigma(D^0) = 0.72 \pm 0.18\ \text{nb}$$
$$2B(D^+ \to K^-2\pi^+)\ \sigma(D^+) = 0.27 \pm 0.05\ \text{nb}$$

with systematic uncertainties of 50%. If $\sigma(D^0)$ is taken as an unknown, then the data is consistent with the statistical-isospin model estimates. However using an independent estimate of $\sigma(D^0)$[39] and the data gives branching ratios slightly smaller than the predictions.[38] For $K_s\pi^\pm$, one expects $2B(D^+ \to \bar{K}^0\pi^+)\ \sigma(D^+) \simeq .35$ nb, using the model and the SPEAR result for $2B(D^+ \to K^-2\pi^+)\ \sigma(D^+)$. A $K_s^0\pi^\pm$ signal this large should be detectable. Thus the data suggests $B(D^+ \to \bar{K}^0\pi^+)$ may be as small as 3 to 5%.[40]

The following sections contain a description of the experimental apparatus, data analysis, and results.

II. Experimental Details

A. Beam

The photon beam is produced using 400 GeV protons at Fermilab. A diagram of the beam line located in the Proton-East Area is shown in Fig. 1.[30,41,42,43,44] Protons strike a beryllium target (305 mm long, 1.5 mm wide, 7.6 mm high). Charged particles are bent into a beam dump by sweeping magnets. The resulting neutral beam is produced at 0° relative to the proton beam line and contains neutrons, photons, K_L^o mesons and other neutral particles. In order to produce a photon beam, a 34 m liquid D_2 attenuator is downstream of the proton target. The D_2 attenuator is surrounded by sweeping magnets to remove charged particles produced by the interaction in the D_2. The neutron to photon ratio is estimated to be reduced by approximately 200 from the production ratio. The detector located in EE-4 is about 120 m downstream of the proton target. The size of the photon beam is determined by a fixed aperture collimator (Coll. 1 in Fig. 1). The aperture used for this experiment gave a 5 cm x 5 cm beam spot in EE-4. Additional fixed and variable aperture collimators reduced the beam halo.

Several steps were taken to reduce the muon flux at the detector. Toroidally wound muon spoiler magnets were placed before and after the proton target. The aperture of some of the sweeping magnets was increased to reduce scraping due to beam halo. Finally steel shielding was added just upstream of the detector area.

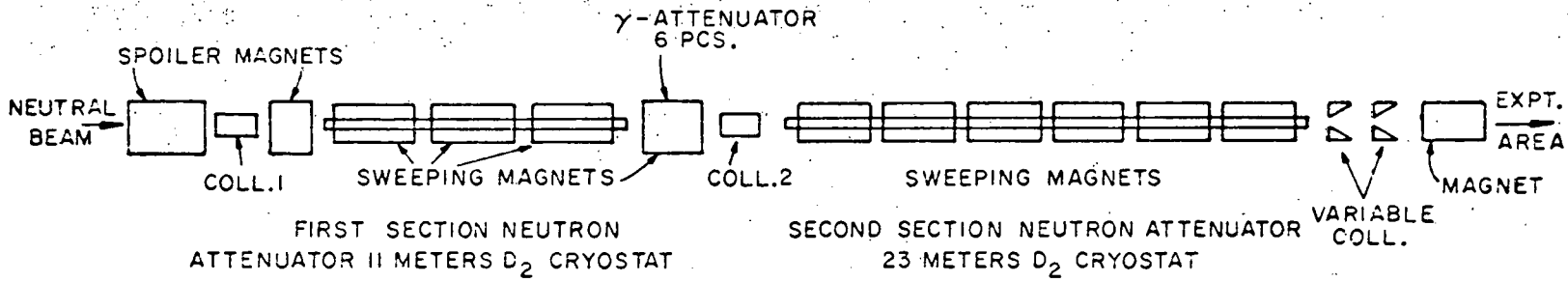

Fig. 1. Neutral Beam Line.

The primary proton beam intensities were typically 6-8 x 10^{11} protons/pulse over a 1 sec spill. The maximum rate of about 2 x 10^{12} protons/pulse was set by the maximum allowed current drawn by the multiwire proportional chambers (MWPC's). The proton intensity was measured using a secondary emission monitor (SEM) located 6 m upstream of the proton target. Targeting efficiencies were monitored using segmented wire ion chambers (SWIC's) and ion chambers. A Wilson-type quantameter was used to measure the photon beam power. The quantameter calibration constant was measured to be 416 ions/GeV.[45]

The resulting photon spectrum is shown in Fig. 2. (See Appendix A.) Backgrounds due to neutral hadrons and the status of the liquid D_2 attenuator could be studied by remotely inserting one to six radiation lengths of lead into the beam.

B. Detector

1. Introduction

The detector, shown in Fig. 3, consists of a magnetic spectrometer, trigger and veto counters, and a particle identification system. The particle identification system includes an electromagnetic shower detector, a hadron calorimeter, and a muon identifier. Table I contains a list of symbols and abbreviations used frequently in the next two sections.

2. Spectrometer

The magnetic spectrometer has five multi-wire proportional chambers (MWPC) and a vertical bending magnet with a field integral of 20 kG-m. The bending magnet gave a 0.595 GeV/c change in

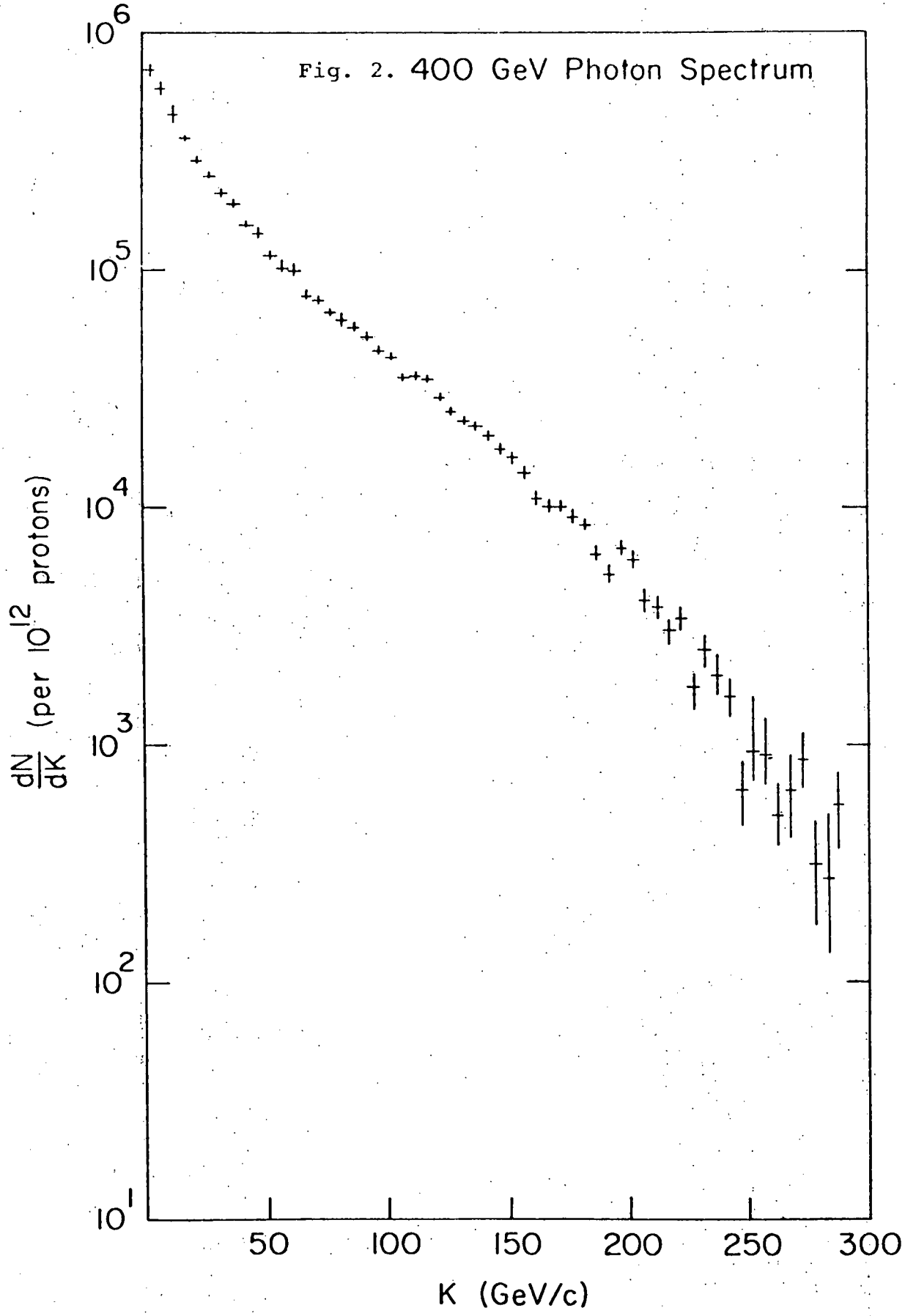
Fig. 2. 400 GeV Photon Spectrum
10^6
10^5
10^4
10^3
10^2
10^1
$\frac{dN}{dK}$ (per 10^{12} protons)
50
100
150
200
250
300
K (GeV/c)

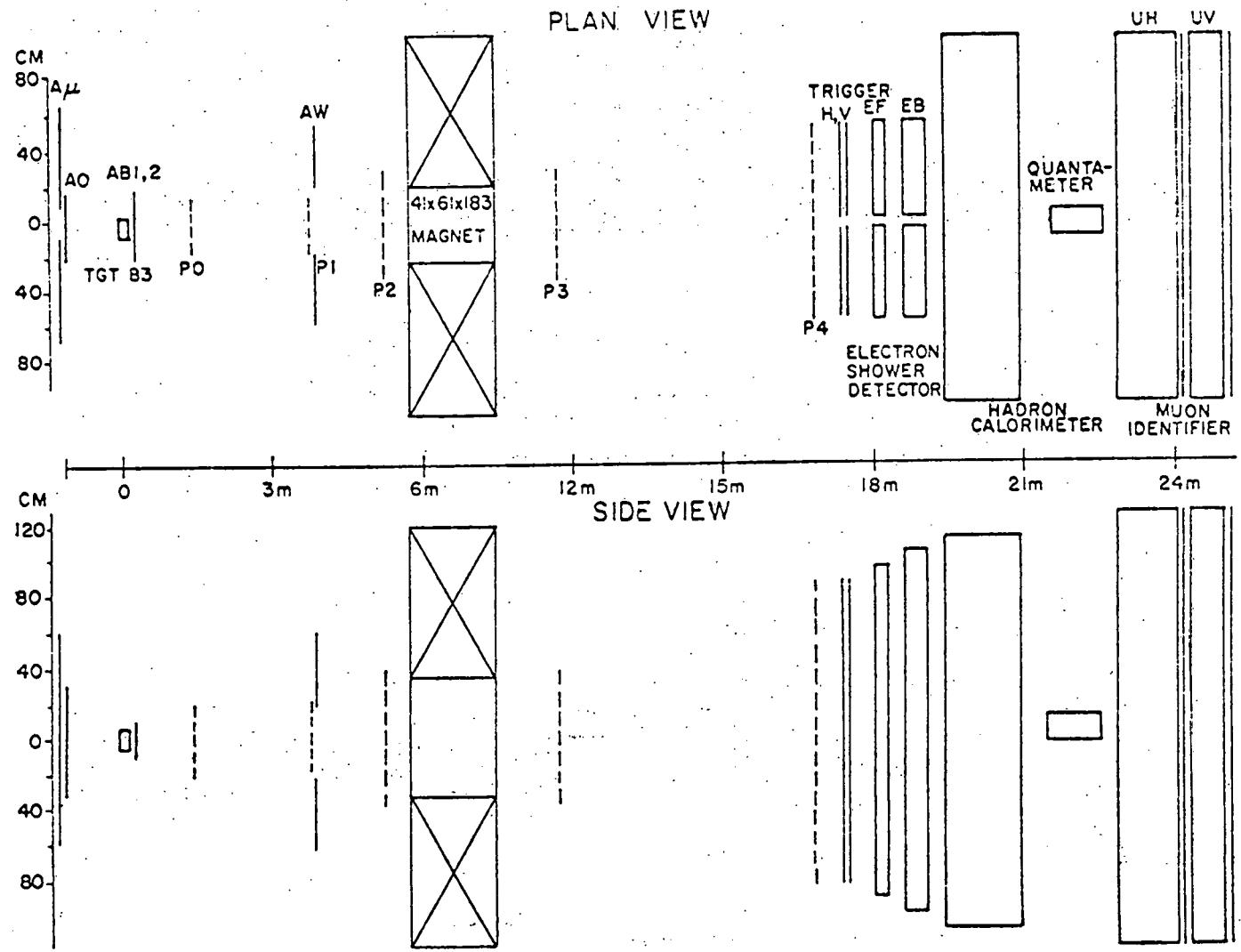

Fig. 3. Apparatus.

Table I: Symbols and Abbreviations

Symbol	Description
AB1, AB2	Wide angle veto counters just downstream of the target
ACE	Data transfer controller
ADC	Analog to digital converter
A_μ + A0	One or more charged particles in veto counters
AW1-4	Wide angle veto counters mounted upstream of the target behind P1
B3	One or more charged particles immediately downstream of the target
CR	Coincidence register
le	le buss line, greater than 7 GeV in either left or right front shower counters
E_{tot}	Energy requirement on sum of hadron calorimeter and shower detector energies
EI	Counter hodoscope just upstream of shower detector (used to avoid π^0's satisfying the le buss line)
EV	Energy in both vertical shower counters
H, V	Horizontal and vertical trigger counters
HC	Hadron calorimeter energy requirement
(L + R)>0	Hits in two H counters and one V counter (or 2V and 1H) used in MG
L · R	Hits in left and right side of MWPC's and H, V array (used in buss lines)
MG	Master Gate
MWPC >0,1,2	Greater than (0,1,2) tracks in multi-wire proportional chambers (P0-P4)
1μ	1μ buss line, hits in at least one μV and μH counter
μH, μV	Horizontal and vertical muon counters
TGI	Trigger input generator
TGO	Trigger output generator

transverse momentum of charged particles. The magnetic field was measured using standard techniques at Fermilab and calibrated absolutely with an NMR probe. Each of the five MWPC (P0 through P4) contains three wire planes, one oriented vertically, and two at ± 11.30 degrees from the horizontal.[44] The wire spacing is 2 mm in all planes except the last vertical plane in P4 which has 3 mm spacings.

3. Trigger and Veto Counters

A variety of scintillation counters were used for fast triggering and vetoing. At the upstream end of the detector about 2 m before the photon target is a vertical array of counters (A0 and A_μ, see Fig. 4). The purpose of these counters is to veto events due to muons or other charged particles not produced in the photon target. The counter A0 is placed directly in the beam and is 61 cm long, 41 cm wide, and 1.6 mm thick. The six A_μ counters surround the photon beam and are 122 cm long, 20 cm wide, and 6.3 mm thick. Three scintillation counters (B3, AB1, AB2) are in a horizontal array 51 cm downstream of the photon target. These counters are 38 cm long, 7.6 cm wide, and 1.6 mm thick. The counter B3 is downstream of the target to detect an interaction which produces forward charged particles. Because of the high rates in B3, the last few dynode stages of the B3 photomultiplier base were connected to an "afterburner" (DC voltage source). AB1 and AB2 are positioned above and below B3. The AB1 and AB2 counters were preceeded by 6.3 mm of lead to convert photons. These counters signal the emission of wide angle particles or showers from π^0. A set of four counters (AW1 through AW4) positioned just outside

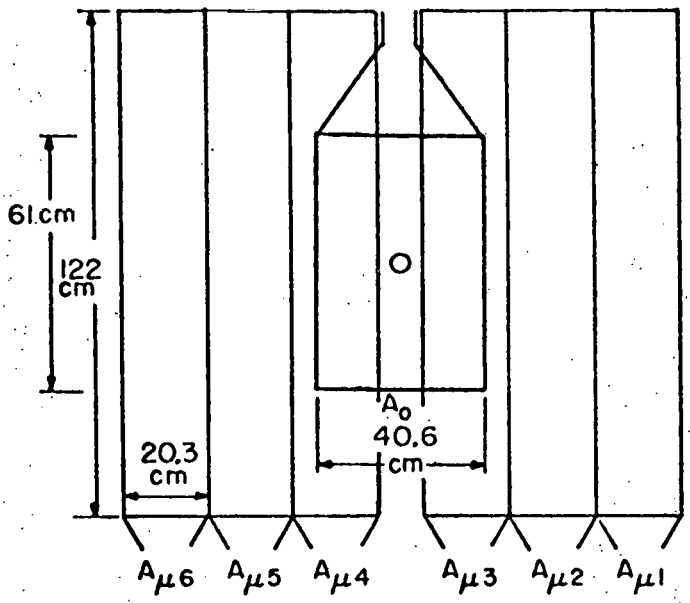

Fig. 4. Upstream View of A0 and Aμ Counters.

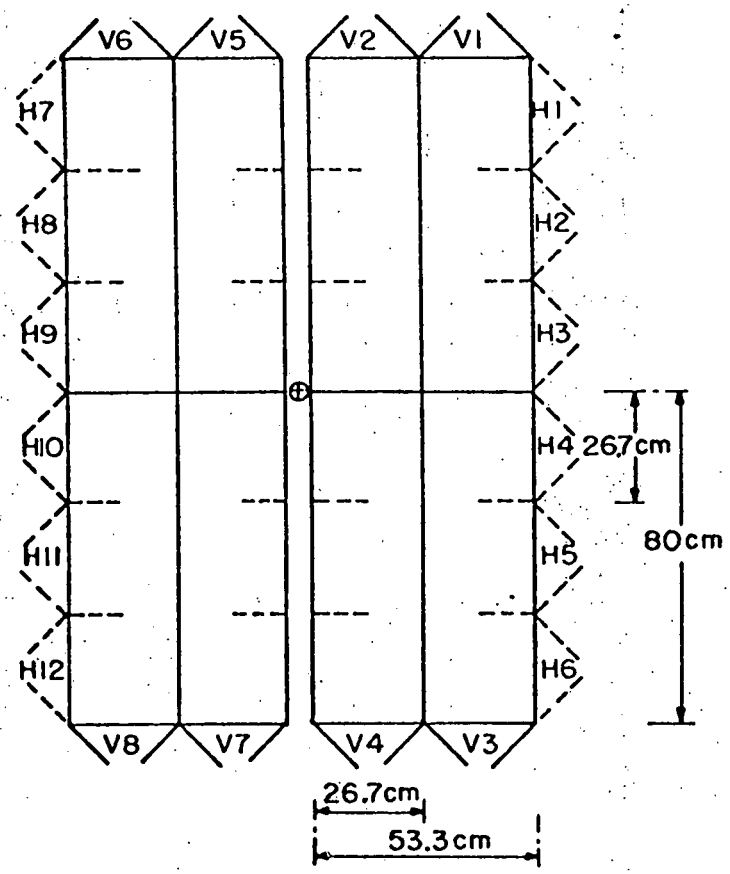

Fig. 5. Downstream View of H and V Counters.

the active area of the chamber P1, signal wide angle charged particles that will not pass through the bending magnet. These counters are 66 cm long, 41 cm wide, and 6.3 mm thick. For triggering purposes we call an event "diffractive" if none of the following counters fired: AB1, AB2, AW1 - AW4. The H and V scintillation counter arrays were made up of twelve horizontal counters and eight vertical counters (shown in Fig. 5). The array has a 6.3 cm wide vertical gap to allow e^+e^- pairs to pass. Together with B3, this array provides the basic fast trigger for this experiment; charged particles from the target of which one or more pass through the detector (H and V array). The H and V counters were provided with an "afterburner" as was B3.

4. Particle Identification System

The particle identification system (Fig. 6) consists of an electromagnetic shower detector[43], a hadron calorimeter, and a muon identifier. The electromagnetic shower detector has forty-six counters containing alternate layers of scintillator (4.8 mm thick) and Pb (6.3 mm thick). The active area of the scintillator in a counter is 51 cm long and 15 cm wide. The shower detector is split into left and right halves to allow the intense vertical band of e^+e^- pairs to pass through the gap. Each side of the detector has a front and rear array of counters. The upstream array has eleven counters each containing six Pb-scintillator layers (six radiation lengths). The downstream array has twelve counters each containing sixteen Pb-scintillator layers (sixteen radiation lengths).

In addition to these forty-six counters, two counters (sixteen radiation lengths) were hung vertically above and below the

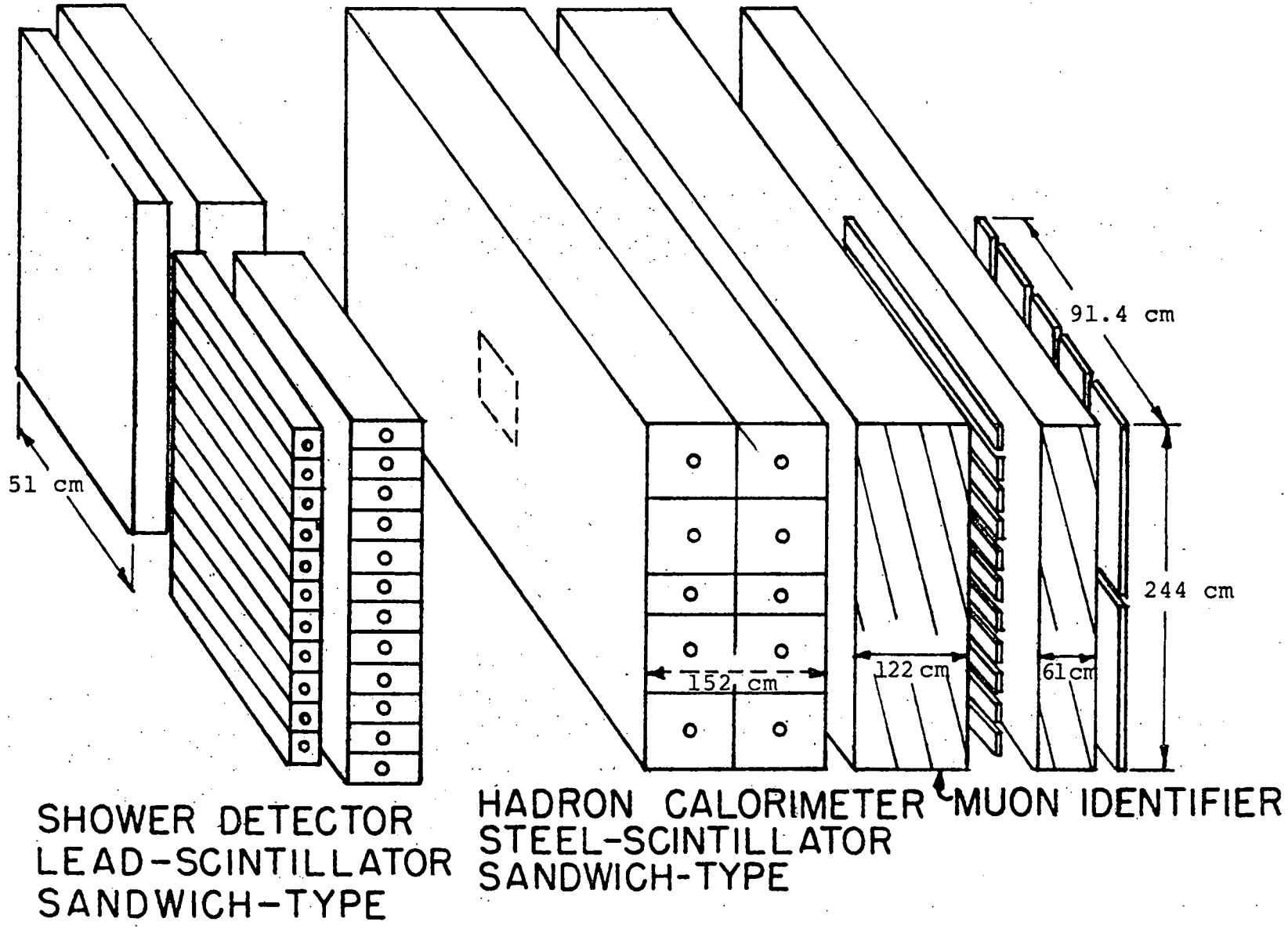

Fig. 6. Schematic of Particle Identification System

beam in the vertical gap. These vertical counters provided some information on electromagnetic showers not contained in the main array and also shielded the part of the hadron calorimeter directly behind the vertical gap. Each scintillator sheet is surrounded by Alzac aluminum for light collection and mechanical support. The scintillator layers are fanned into a lucite mixing block through lucite light pipes. Several steps were taken to improve light collection uniformity. A yellow filter was placed between the mixing block and the photomultiplier (58 AVP). Yellow light is attenuated much less in scintillator than, say, violet to UV light, therefore the yellow filter improves light collection uniformity. The 11 cm diameter photomultiplier tubes have non-uniformities of 30% across the face of the tube. This is reduced to a 5% effect by aligning the axis of maximum uniformity of the tube with the axis of shower development. The shower counters were calibrated using special e^+e^- runs (see Appendix A). A light pulser system monitored the stability of the detector.

Scintillation counters (EI 1-10) are placed directly upstream of the shower detector and mask the active area of the central five front shower counters on each side of the beam. A charged particle is required in the matching EI counter before the corresponding shower counter is included in the shower counter energy requirement used in various trigger requirements (le for example, see Section II.C.2). In this way false single electron triggers caused by neutral pions ($\pi^o \rightarrow \gamma\gamma$) are avoided. The EI counters cover only the central horizontal region of the shower counters which view the target directly (hence those counters which may contain photons

from the π^0 decay).

The hadron calorimeter has twenty-four sheets of steel 180 cm wide, 200 cm high, and 4.5 cm thick interspaced with 6.3 mm sheets of scintillator. There are twenty counters, ten on each side of the beam, stacked five high and two deep (only sixteen were in use for this experiment). Each counter has twelve sheets of scintillator connected to a single photomultiplier (58 AVP). Sixteen of the counters have scintillator sheets 89 cm long, 46 cm wide, and 6.3 mm thick. Four counters have scintillator 89 cm long, 15.2 cm wide, and 6.3 mm thick. The steel sheets have a 15 cm square hole to allow the beam to pass through.

The muon identifier consists of a steel shield 122 cm thick, a horizontal array of twenty-two scintillation counters (μH), another steel shield 61 cm thick, and a vertical array of eighteen scintillation counters (μV). Each of the μV (μH) counters is 122 cm (91 cm) long, 20 cm wide, and 6.3 mm thick. An additional muon counter (μH-23) was placed downstream of the main array in the beam line and shielded by roughly the same amount of steel. The muon counters were connected to 8575 photomultiplier tubes.

C. Electronics

1. Data Acquisition System

A diagram of the electronics is shown in Fig. 7. This system must receive signals from various types of detectors, choose potentially interesting events and write them onto magnetic tape without introducing large deadtimes. Event selection is done on two levels. First, a fast trigger (master gate) based on coinci-

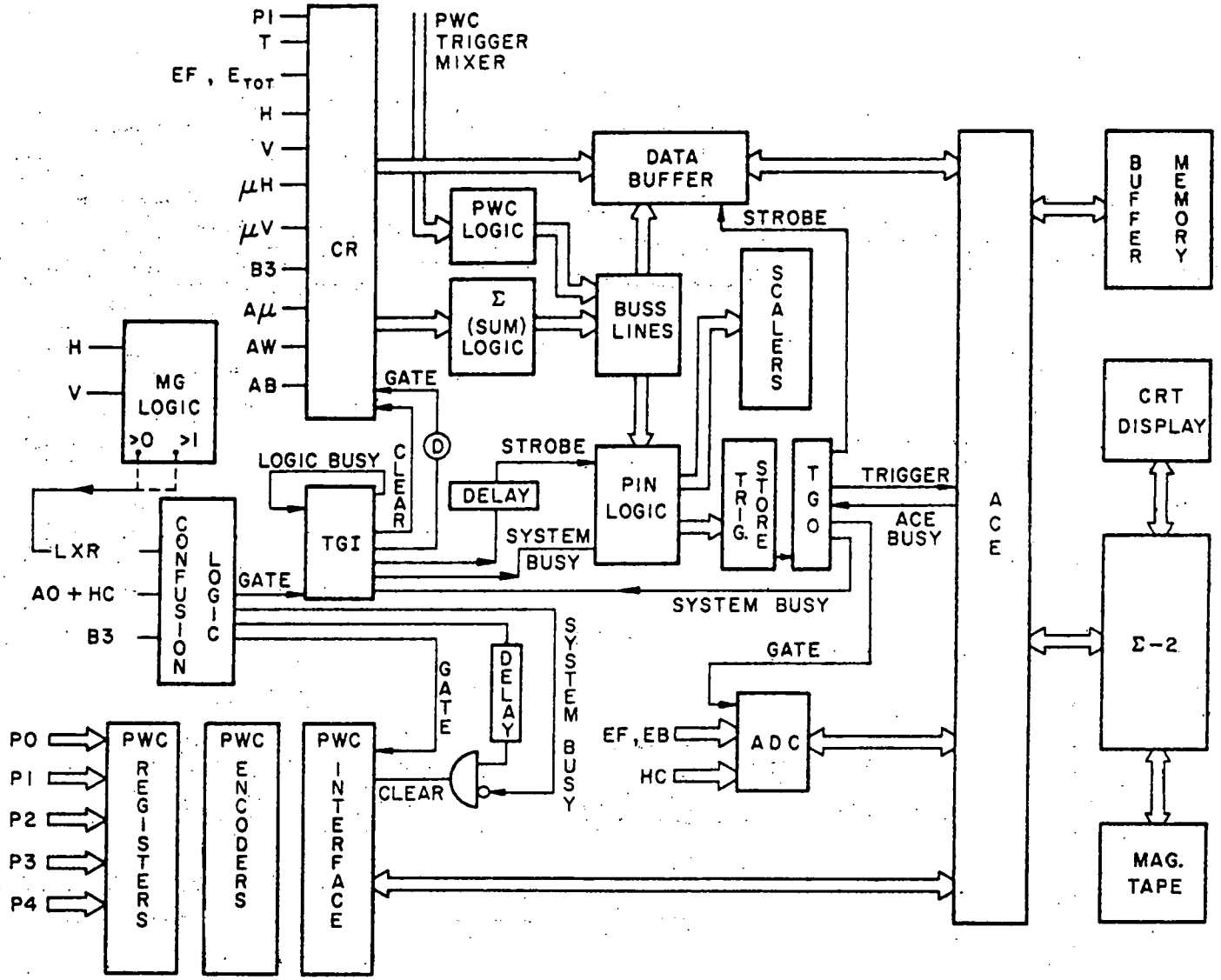

FIG. 7. ELECTRONICS BLOCK DIAGRAM.

dences between scintillation counters and/or pulse height requirements is generated. The trigger is made as loose as possible without introducing large deadtimes. The second level of event selection is done using DC (Nevis) logic. In this way up to sixteen types of events with sixteen different requirements (buss lines) may be selected. The events chosen are written onto magnetic tape by the Sigma-2 computer. The remainder of this section will follow the event selection process through in more detail.

The master gate logic is shown in Fig. 8. The presence of two or more particles at the rear of the spectrometer is indicated by a coincidence in the H and V counter hodoscope. The outputs of all the H and V counter discriminators are fanned into sum modules which give >0 and >1 outputs for each array (H and V). Two particles must intersect a minimum of two H counters and one V counter (or two V counters and one H counter) to form (L + R) >0. The counter B3 indicates a charged particle from the target. The counter A0 indicates a charged particle in the beam or beam halo. HC implies that a minimum of about 40 GeV of energy was deposited in the hadron calorimeter.

The inputs to the "confusion logic" are (L + R) >0, B3, and (A0 + HC). The confusion logic generates a >1 output if any two of the three inputs are satisfied and if:

1) No previous input for 100 ns,

2) No output for 250 ns,

3) No external veto.

Similarly a >0 output is generated if any one of the three inputs

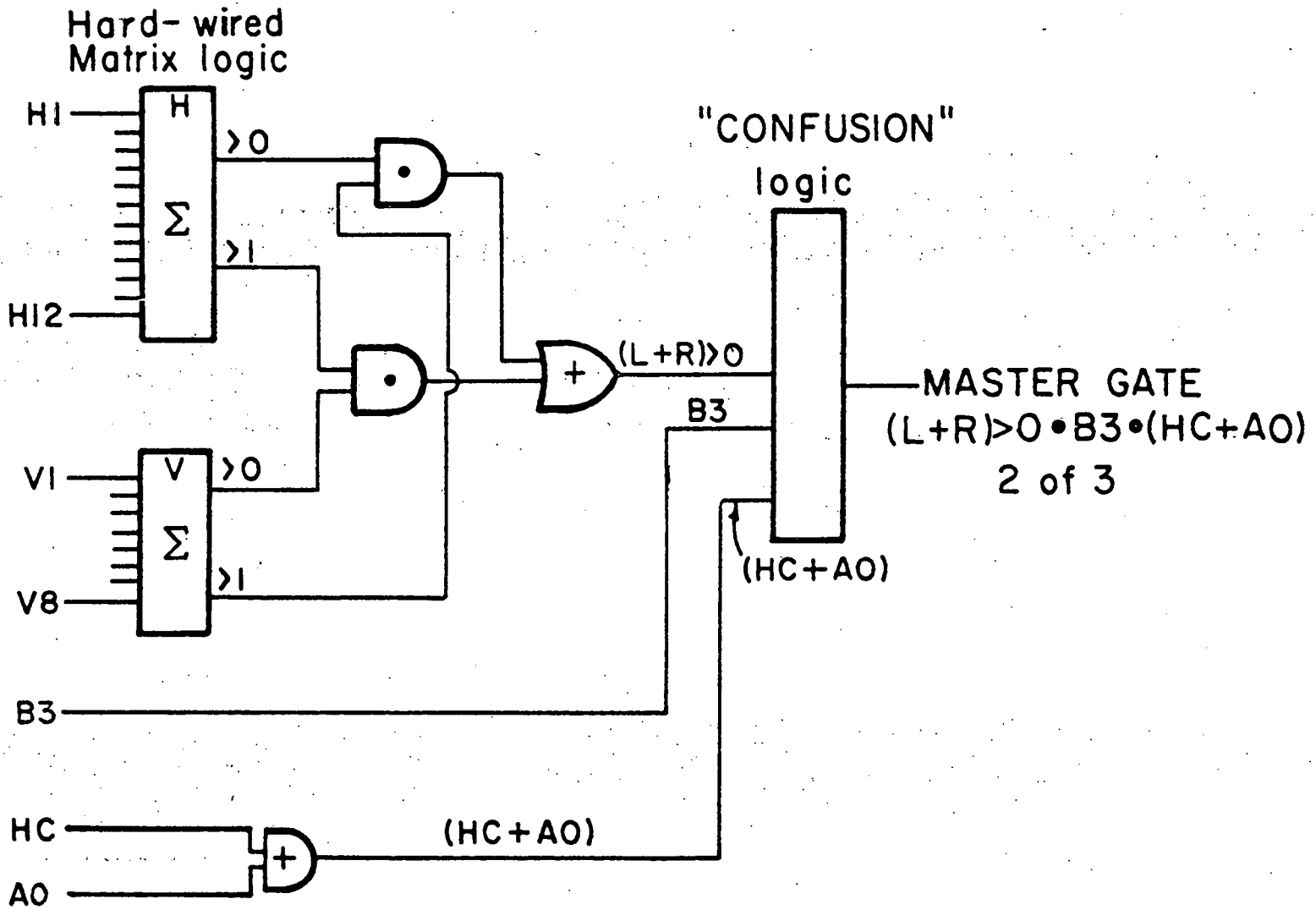

Fig. 8. DERIVATION OF MASTER GATE

is satisfied. The master gate is formed from the >1 output of the confusion logic. The first requirement helps to reduce deadtime due to a large flux of particles hitting the target in a short time (bad spill structure) or charged particles in the beam. This is why A0 is included in the master gate. The second requirement insures that master gates will not be sent to the DC logic while it is still busy. The external veto stops any master gate from occurring while the Sigma-2 is reading out an event or while the DC logic is waiting for readout. Most of the data satisfied the standard two or more charged particle trigger (B3 * (L + R)>0). The trigger (B3 * HC) indicates one or more charged particles from the target which pass through the gap in the H and V array, but leave significant energy in the hadron calorimeter. The trigger (HC * (L + R) >0) is a strange particle trigger (K^0_S, Λ, etc.). In this case a neutral particle decays downstream of the B3 counter and satisfies the HC and (L + R) >0 requirement, but not B3. In addition to sending out a master gate, the confusion logic sends a clear and gate to the MWPC interface and also keeps track of logic livetime. If the DC logic decides to keep the event, the clear pulse is delayed, otherwise the MWPC registers are cleared. The confusion logic >0 and >1 outputs are scaled for all outputs (no logic deadtime) and for those outputs sent to the DC logic, this ratio (>1 with deadtime/>1 without deadtime) gives the logic deadtimes.

The >1 output from the confusion logic is sent to the trigger input generator (TGI). The TGI sends a clear and delayed gate to the coincidence registers, and a strobe for the pin logic. Each

time the TGI accepted a trigger, a logic deadtime was generated to prevent accepting another input trigger during the time needed to propagate the DC logic, make output triggers and store the event into the data buffers.

The coincidence registers (CR) which generate DC latches contain information from scintillation counters, dynode signals from the shower detector and hadron calorimeter, and trigger mixer signals from the MWPC's. Once the CR's are filled, no further time coincidence operations are needed. The outputs from the CR's go to the CR logic system and the data buffer. The CR logic system provides up to sixteen logical definitions which are then distributed to a data buss (buss lines) to which sixteen independent pin logic modules connect. Each of the sixteen pin logic modules defines a trigger type according to internal connections corresponding to true, false, or don't care for each of the sixteen buss lines. The TGI sends a delayed strobe to the pin logic modules. The outputs of each of the pin logic modules are sent to the trigger output generator (TGO) where they are or'ed together to form an output trigger. Each of the trigger types from the pin logic can be "prescaled" so that the mixture of trigger types can be controlled. Separate outputs from the pin logic modules (not prescaled) are sent to scalars.

After receiving the event trigger, the TGO sends out gates for the pulse height digitizers (ADC's) and a strobe for the data buffer to save the event for readout. At the same time, the TGO sends a read pulse to the data transfer controller (ACE) and generates a system deadtime which is extended by the readout

system to allow the event data to be transferred to the buffer memory. During system deadtime the TGI accepts no input events and holds the MWPC clear. After the event data is transferred to the buffer memory, ACE signals the system is ready for another event. This process continues until either the buffer memory is full or an end of spill signal is received. At this time an interrupt is sent to the Sigma-2 computer which reads in the events from the buffer memory and writes formatted data onto magnetic tape. Each data event is about 150 (16-bit) words long and the buffer memory capacity is 32K. Therefore, we may take approximately 200 events per pulse before the memory fills up. Since the beam spill repetition rate was about ten seconds, the Sigma-2 is free to act as a monitor when it is not busy writing data onto magnetic tape. A main foreground program formats data written on tape, fires the light pulser, and accumulates statistics on beam monitors and pin logic types. Pulse height information from each shower counter and a monitor photodiode was written on magnetic tape and printed out at the end of each run (data tape) along with the other information accumulated by the foreground program. A background program which ran while the foreground program was idle analyzed a sample of events. Various distributions and individual events could be displayed on the on-line CRT display. The background program also accumulates information on the number of tracks per event, MWPC efficiencies and average hits per plane, trigger types and hit patterns in the H x V hodoscope. This information is also printed out at the end of each run.

2. Single Lepton Event Triggers

In this section, the single lepton triggers (Pin logics 1e and 1μ, see Fig. 9) will be discussed. These are only two of a variety of triggers (pin logics) used in this experiment.[45]

The single muon trigger (Pin logic 1μ) had the following buss line requirements: $\overline{A0 + \Sigma A_\mu}$, $\overline{AB + AW}$, $\overline{\bar{L} \cdot \bar{R} \cdot EV}$, MWPC >1, L · R, 1μ and E_{tot} > Lo, where a $\bar{X}$ means veto on X. The counters A0 + ΣA_μ veto counters with charged tracks in or around the beam upstream of the target. The counters AB + AW veto events in which one or more wide angle particles do not pass through the detector as discussed in section II.B.3. We refer to events in which there are no hits in counters AB1, AB2, or AW1-AW4 as "diffractive" events. In the MWPC readout system eight wire signals connect to an amplifier card which sends outputs to the MWPC coincidence register. In addition, each card provides an "OR" output of the eight wires. The "OR" or trigger mixer signals were used in the buss lines containing MWPC information. A schematic of the MWPC >0, >1, and >2 buss lines is shown in Fig. 10, where $>0^3$ stands for at least one hit in each of the three MWPC planes (u, v, x) and $>1^2$ ($>2^2$) stands for at least two (three) hits in two of the three planes. Therefore the MWPC >1 requirement eliminates events where there is no chance of reconstructing more than one track. The trigger mixer signals are also used to form an "OR" of larger groups of wires. For example all the wires in the x-plane to the left of the beam region can be grouped into a L "OR" output. A central vertical band of wires is omitted to avoid Bethe-Heitler e^+e^- pairs just as the H and V counters are split. These outputs

FIG. 9. TYPICAL PIN LOGICS FOR PHOTON RUNNING.

BUSS LINE \ PIN LOGIC	2e	1e	μe	2μ	2μ	1μ	2π	4π	Monitor Pins			2π Hi
$A_O + A_\mu$	×	×	×	×	×	×	×	×				×
$A_W + A_B$		×				×	×	×				×
$\overline{L} \cdot \overline{R} \cdot EV$					×	×	×	×				
MWPC>0											✓	
MWPC>1	✓	✓	✓	✓	✓	✓	✓					
MWPC>2								✓				
$\overline{L \cdot R}$	×	×			×	×						×
2μ				✓	✓							
1μ			✓			✓						
2e	✓											
1e		✓	✓									
E_{TOT}>Lo					✓	✓	✓	✓				
E_{TOT}>Hi		✓										✓
PS>0									✓	✓	✓	
$EV_1 \cdot EV_2$										✓		
$EV_1 + EV_2$				×					✓			

✓ Required in coincidence

× Required in anti-coincidence

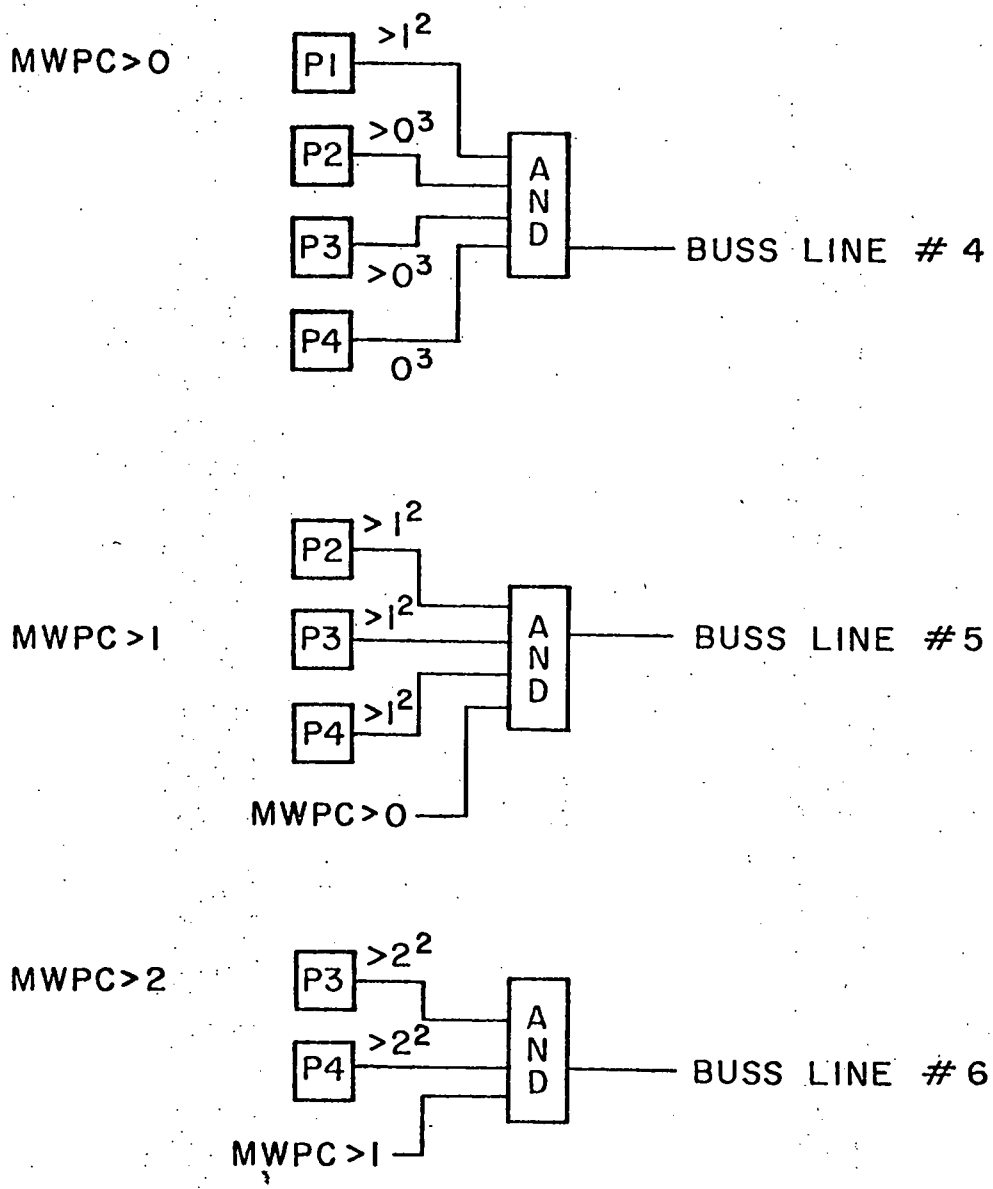

Fig. 10. MWPC >0, >1, >2.

along with information from the H and V counter array are used to form the buss lines $L \cdot R$ and $\bar{L} \cdot \bar{R} \cdot EV$. $L \cdot R$ requires at least two particles in the detector, one on each side of the central vertical gap. EV stands for EV1 + EV2 where EV1 and EV2 are the vertical shower counters. The $\bar{L} \cdot \bar{R} \cdot EV$ veto eliminates events with more than 7 GeV deposited in the vertical shower counters and no tracks outside the beam region. Events of this type are likely to be Bethe-Heitler e^+e^- pairs. The 1μ buss line is satisfied if there are one or more muon counters on in each of the two planes of counters (μV and μH). E_{tot} is formed from the addition of dynode signals from the shower detector and hadron calorimeter. The Lo threshold corresponds to about 15 GeV deposited in the shower counter and hadron calorimeter. This requirement eliminated events that have a large fraction of their tracks (energy) missing the active area of the detector. The single muon trigger requires basically two or more particles in a "diffractive" event with at least one muon counter in each of the two planes firing.

The single electron trigger (Pin Logic 1e) had the following buss line requirements: $\overline{A0 + \Sigma A_\mu}$, $\overline{AB + AW}$, $L \cdot R$ (or $\overline{\bar{L} \cdot \bar{R} \cdot EV}$), MWPC >1, 1e, and E_{tot} > Hi. After about one-half of the data taking period $L \cdot R$ was replaced by $\overline{\bar{L} \cdot \bar{R} \cdot EV}$. This had a slight effect on overall trigger rates. The E_{tot} >Hi corresponds to about 40 GeV. The 1e buss line used dynode signals from the front bank of the shower counters to require greater than 7 GeV in either the left or right front bank (EFR + EFL). The central front shower counters were gated by the EI counters as discussed in section II.B.3. Thus the single electron trigger

requires two or more particles in a "diffractive" event with evidence for activity in the shower detector. The effect of making these trigger requirements is given in section III.

III. Data and Results

A. Overview

In this section the results of a search for the photoproduction of a pair of charmed D mesons are presented. This experiment is able to identify neutral V^0's (K_S^0, Λ, $\bar{\Lambda}$) and leptons, but not charged pions, kaons, or protons. We have searched for the reaction

$$\gamma + Be \rightarrow D\bar{D} + X$$
$$\hookrightarrow \text{leptons} + \ldots$$
$$\hookrightarrow K_S^0 \, n\pi^{\pm}$$

where X could include pions or photons from the production of D^*'s. The K_S^0 and lepton are identified and all other tracks are assumed to be pions. The invariant mass spectrum for $K_S^0 \, n\pi^{\pm}$ (n = 2-6) is calculated. We then look for an excess of events near the D meson masses. Details of K_S^0 and lepton identification, background studies, and the results of the search are presented.

B. Data Selection

The raw data tapes written by the on-line computer were reanalyzed to reconstruct the tracks in the detector. At this point the data is a mixture of many trigger types (single lepton, dilepton, hadronic, and monitor triggers). First, all events containing K_S^0's were selected. Second, events with lepton candidates were selected from the K_S^0 events.

The following cuts were made to select the K_S^0 events of interest:

1. A neutral V^0 identified as a K_S^0

2. Two or more additional charged tracks which verticize within ± 12.7 cm of the center of the target along the beam direction
3. Four to eight tracks
4. No prongs
5. Total energy of all charged tracks less than 300 GeV

A V^0 is defined as a pair of oppositely charged tracks which verticize more than 62 cm downstream of the production target. The V^0 track vector is required to intersect the main vertex within the production target. (See Fig. 11). The V^0 is identified as a K_S^0 if the mass of the two tracks (assuming both are pions) is 498 ± 10 MeV. The minimum number of tracks of interest is four, since we must have a lepton, a K_S^0 which decays into two pions, and at least one other track to form the $K_S n\pi$ mass spectrum. The total number of tracks is required to be less than nine to reduce the number of combinations in $K_S^0 n\pi$ mass plots and to reduce the number of neutron induced events. Since the neutron energy spectrum peaks at energies above 300 GeV for 400 GeV incident protons and the number of photons with energy greater than 300 GeV is small, we require the total energy of the tracks to be less than 300 GeV. A "prong" (or stub) is defined as a track which passes through the chambers upstream of the spectrometer magnet, but does not pass through the chambers downstream of the magnet. This no prong cut is included to be consistent with the "diffractive" trigger requirement ($\overline{AW + AB}$) introduced in the lepton triggers used in the next set of cuts. The effect of excluding events with wide angle particles which miss the detector is included in the Monte

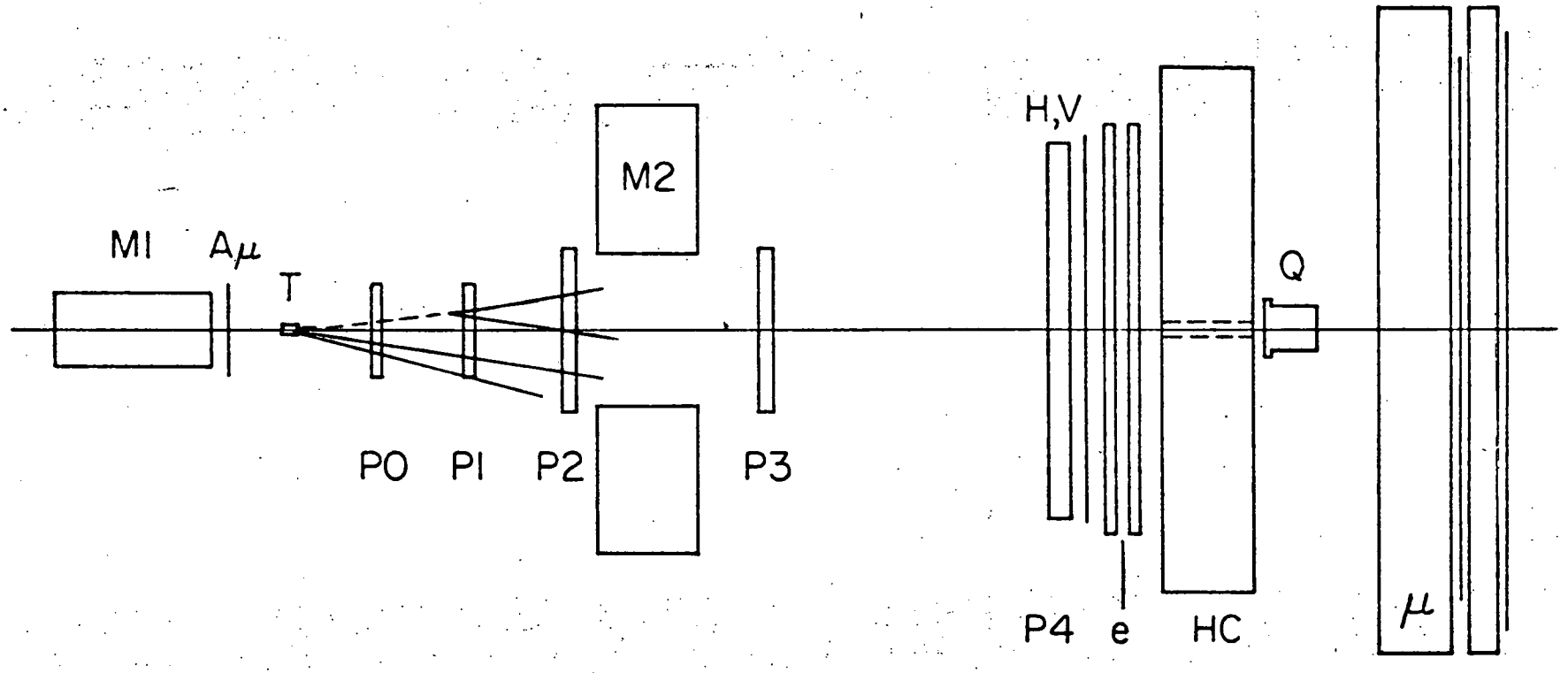

Fig. 11. Schematic of K_S^0 Decay in Detector.

Carlo calculation of the acceptance used to determine cross-sections (Section IV.A). The K_S^0 mass spectrum for the 84,000 events passing these cuts is shown in Fig. 12. In Fig. 13 we show the $K_S^0 2\pi$ mass spectrum to illustrate the continuum of events we observe in $K_S^0 n\pi$ mass spectra before the lepton cuts are made.

From this sample of K_S^0 events, we want to select events of the form $K_S^0 n\pi^{\pm}$ + lepton + other tracks where n = 1-4. We first require the lepton trigger (Pin logics 1e and 1μ) and then require additional cuts for leptons to be satisfied.

Applying the single muon trigger reduces the 84,000 K_S^0 events to 3,400 events. The single muon trigger requires a single muon counter in each plane (horizontal and vertical) of the muon counter array, but does not match a track with the two muon counters. We therefore require the track of the muon candidate to project to within the radius of search of one muon counter in each plane. The radius of search was taken to be three times the root-mean-squared displacement expected from multiple scattering. This cut left 1,200 muon candidates from the K_S^0 data sample.

Applying the single electron trigger reduces the 84,000 K_S^0 events to 22,000 events. For an electron candidate we require (1) that almost all of its energy be deposited in the shower counter and, (2) that it has the longitudinal shower development characteristic of an electromagnetic shower. The data sample is reduced to 2,000 events by the following cuts:

1. $.8 < E/p < 1.2$ where E/p = shower counter energy/track momentum
2. $.5 < f < 1.5$ where

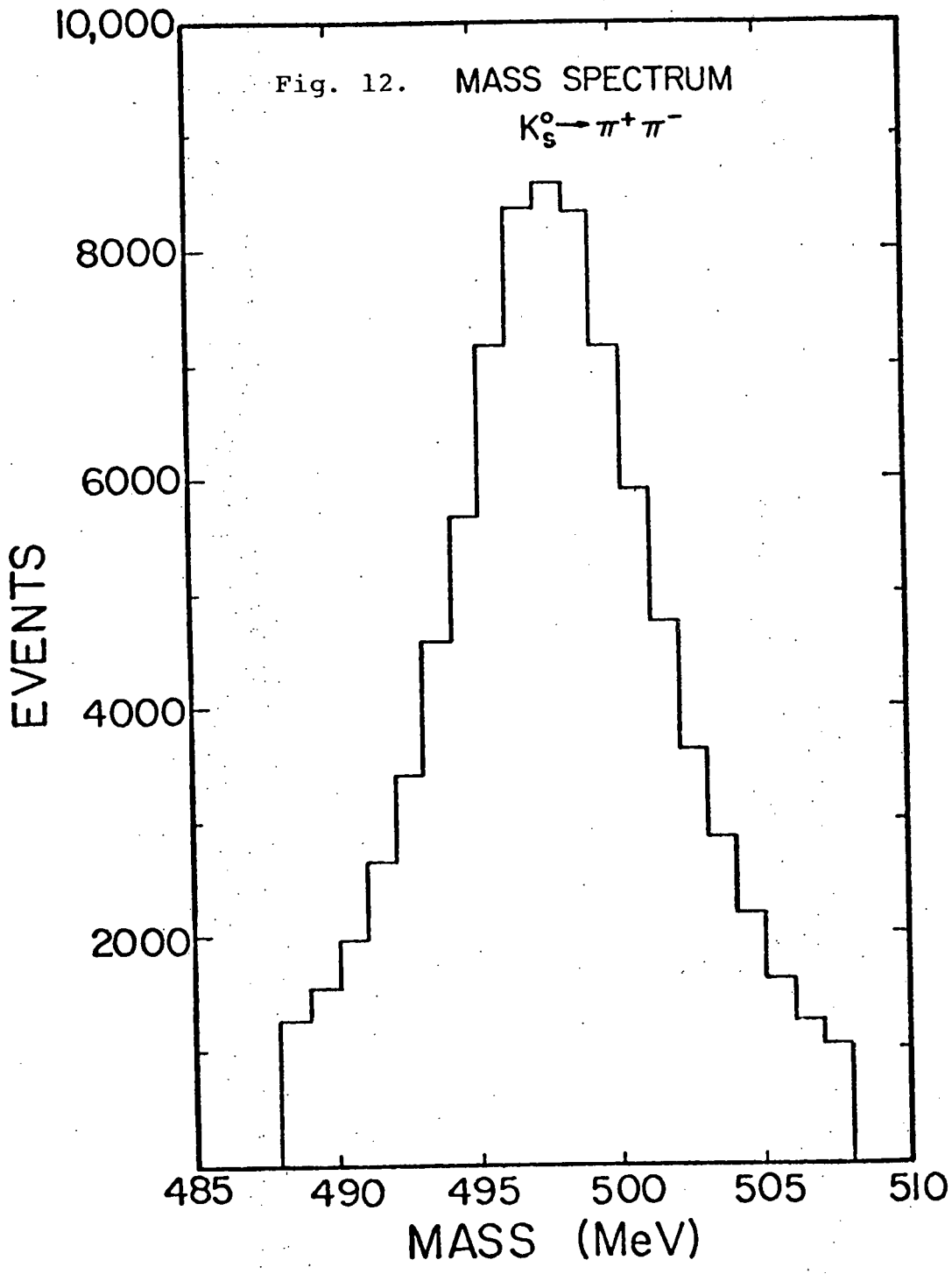
10,000
8000
6000
4000
2000
EVENTS
485
490
495
500
505
510
MASS (MeV)
MASS SPECTRUM
$K_s^o \rightarrow \pi^+ \pi^-$

Fig. 12.

Fig. 13.

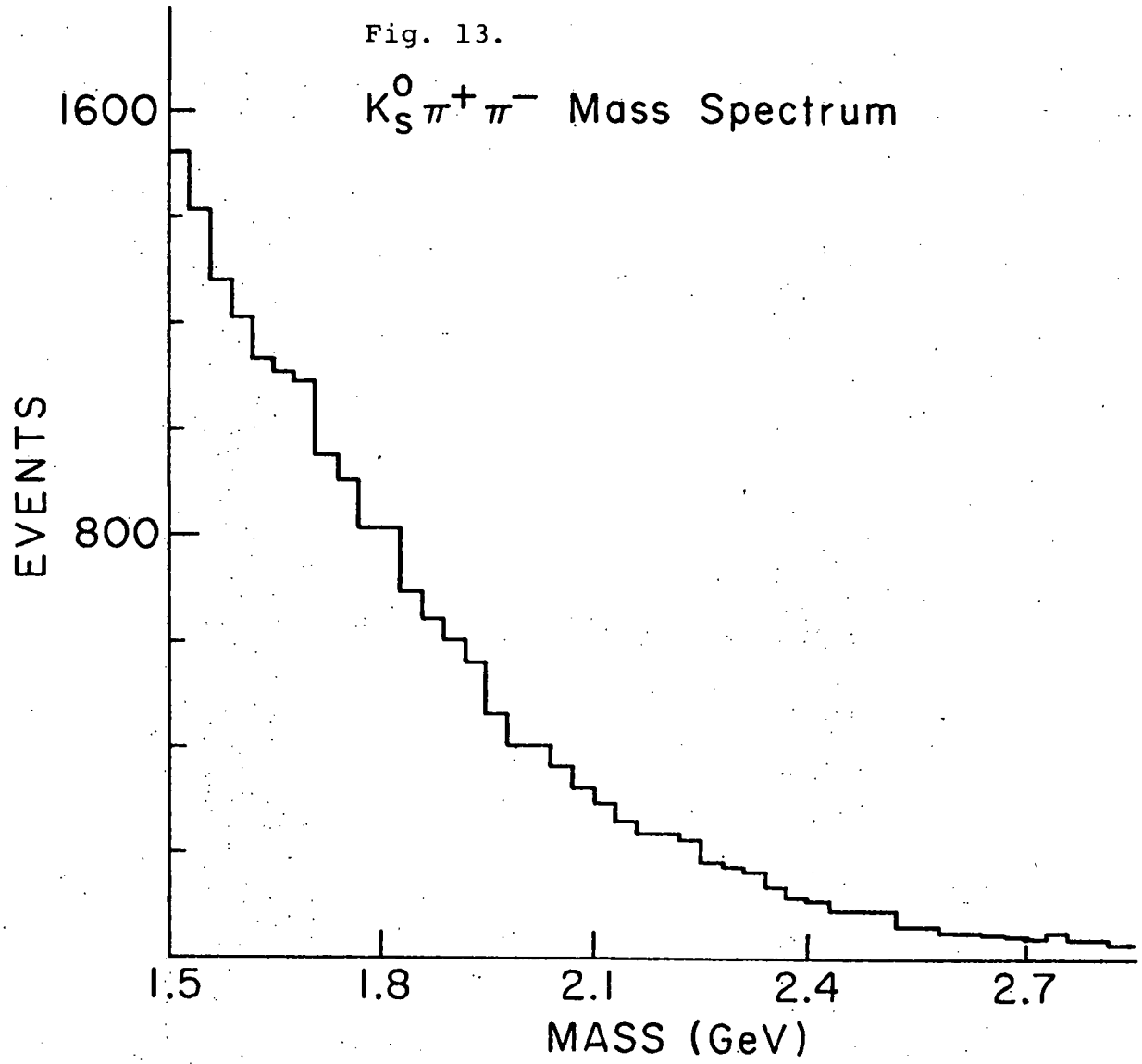

$$f \equiv \frac{1}{N} \ln\left(\frac{p}{.022\ \text{GeV}}\right)\left(\frac{E_F}{E_F + E_B}\right)$$

N = normalization constant to put the peak of the f distribution at 1.0

p = track momentum measured by spectrometer

$E_{F(B)}$ = energy deposited in the front (back) shower counters associated with the track

The momentum dependence of $\left(\frac{E_F}{E_F + E_B}\right)$ is removed by the term $\ln\left(\frac{p}{.022\ \text{GeV}}\right)$. The average amount of energy deposited in the front shower counters (six radiation lengths) is inversely proportional to the shower maximum at that energy, where $\ln\left(\frac{p}{.022\ \text{GeV}}\right)$ is the position of the shower maximum in radiation lengths. The effectiveness of these cuts in rejecting hadrons in two track events can be determined by comparing pions from the decay $\rho(770\ \text{Mev}) \rightarrow \pi^+\pi^-$ to electrons produced in special spectrum and shower counter calibration runs (Appendix A). The E/p and f distributions are shown for electrons and pions in Figures 14 and 15.

At this stage of the analysis we see no evidence for a large K^o_S-lepton correlation based on the number of events in the final data sample (see Section III.D).

C. Results

The results of the preceeding analysis gives the final muon-K^o_S and electron-K^o_S data samples. To look at the data in a more sensitive way, we now calculate the invariant mass spectrum for the $K^o_S n\pi$ combinations. The formula used to calculate the invariant mass (M) is $M^2 = \sum_{ij}\sum m_{ij}^2$ where i and j range from one to the total number of tracks and $m_{ij}^2 = m_i^2 + m_j^2 + 2E_iE_j - 2\vec{p}_i \cdot \vec{p}_j$.

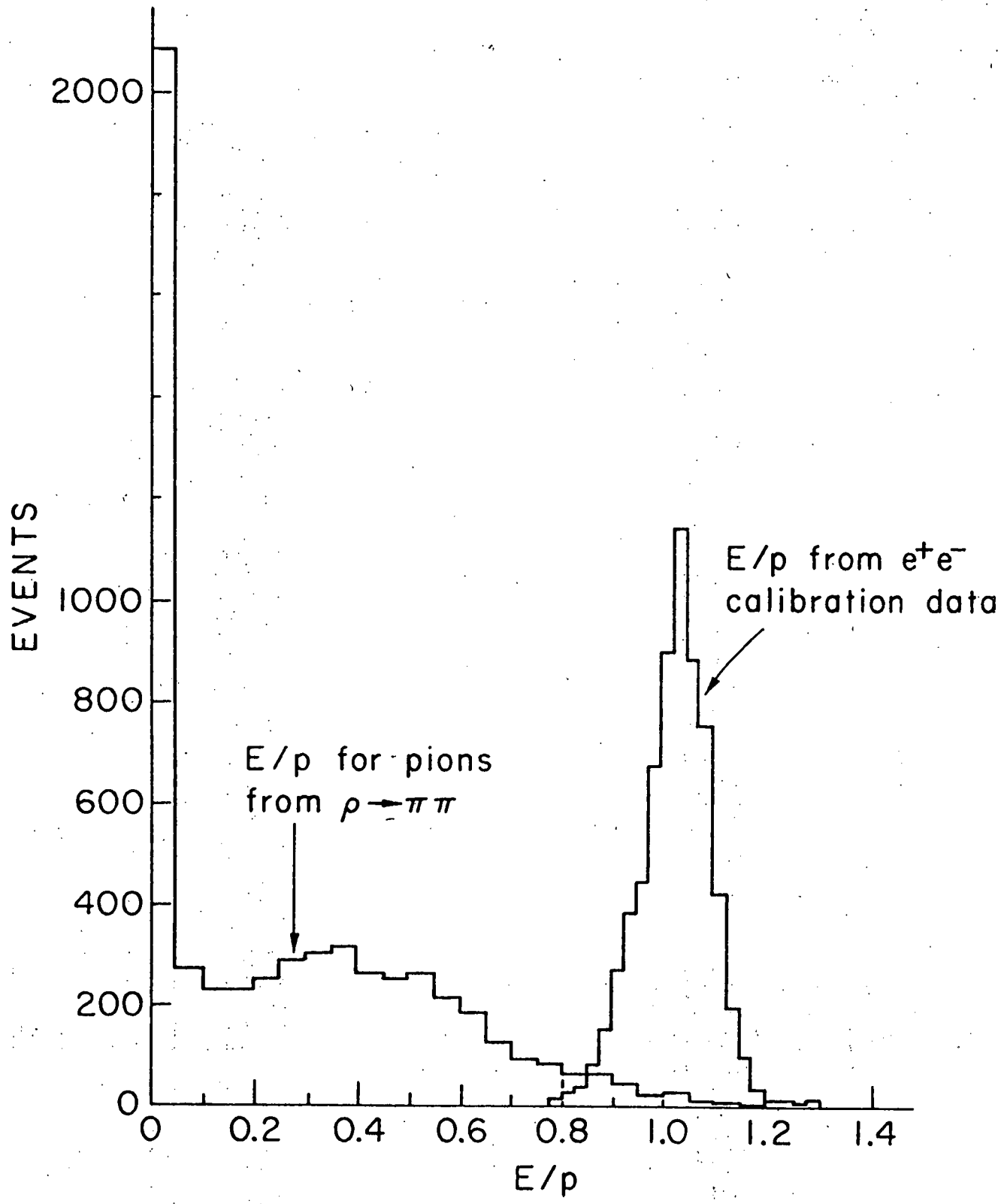

Fig. 14. E/p Distributions.

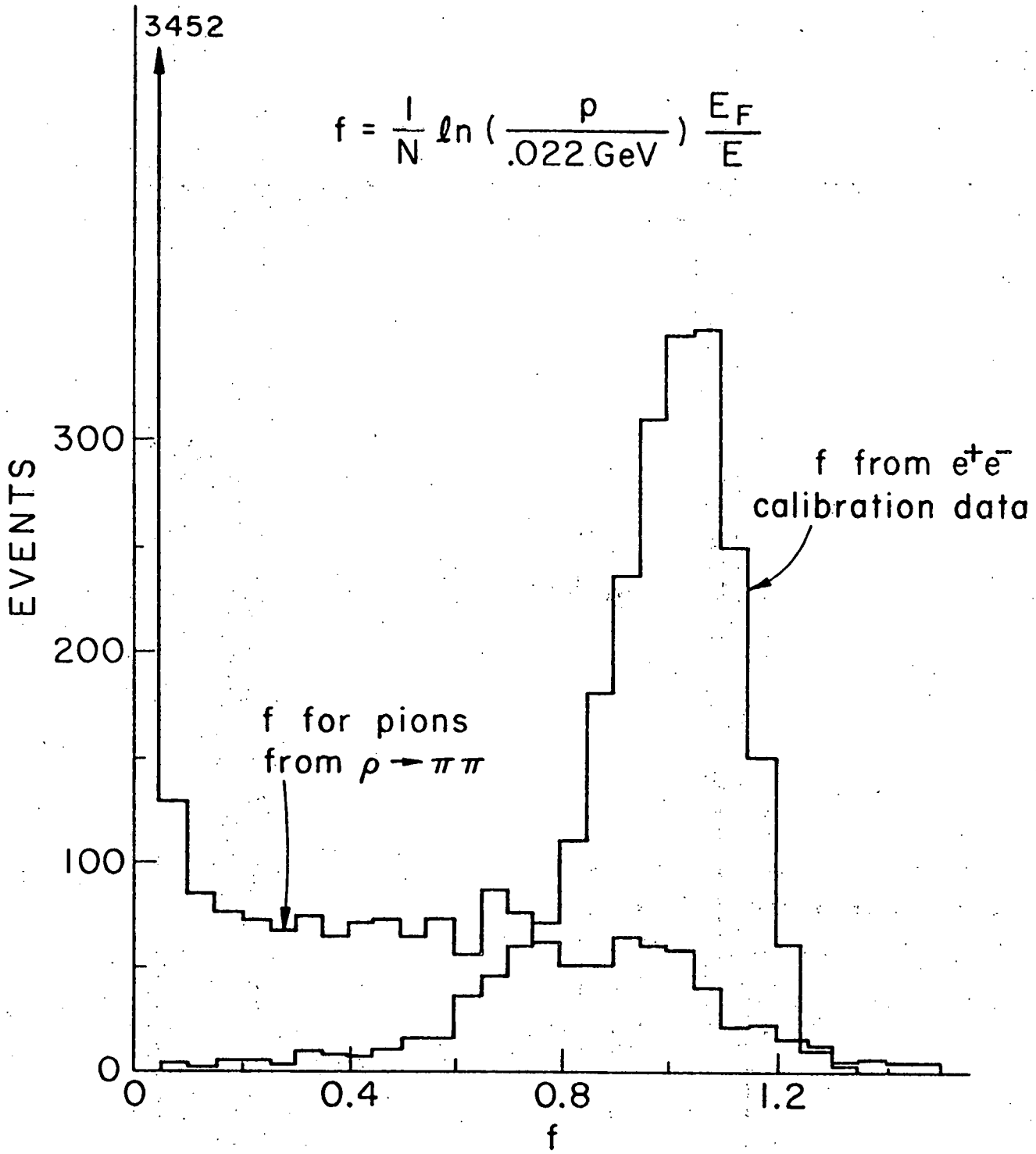

Fig. 15. f Distributions.

The resulting mass spectra are shown in Figures 16-19. If there had been appreciable $D\bar{D}$ production accompanied by semileptonic decays in our data, we should have seen an accumulation of events at the D mass. We see no evidence for peaks in the mass spectrum near the D mass. There is a small peak in $K_S 4\pi$ in the electron sample, however the number of events is not statistically significant (compared to the number of events in adjacent bins).

D. Backgrounds

The background is a combination of both photon and non-photon induced events with one of the tracks misidentified as a muon or an electron. We attribute the non-photon induced events to neutral hadrons (predominantly K_L^o's) in the neutral beam. In this section we discuss, first, the number of background events we expect from lepton misidentification and finally, what fraction of these events are photon induced.

The fraction of events misidentified as leptons can be determined by looking within the data sample of K_S^o events. The fraction of the tracks from the K_S^o identified as leptons is measured and attributed entirely to misidentification, or, in the case of muons, decays in flight. The measured π/μ rejection is 7.3×10^{-3} per track. This agrees with an estimate of the π/μ rejection which assumes all muons are from pion decays. Using $c\tau$ of the pion and the length of the pion decay path gives a π/μ rejection of approximately 10^{-2}. The π/e rejection measured using the tracks from the K_S^o decay is 1.8×10^{-2} per track. The total number of events we observe in the final lepton-K_S^o data

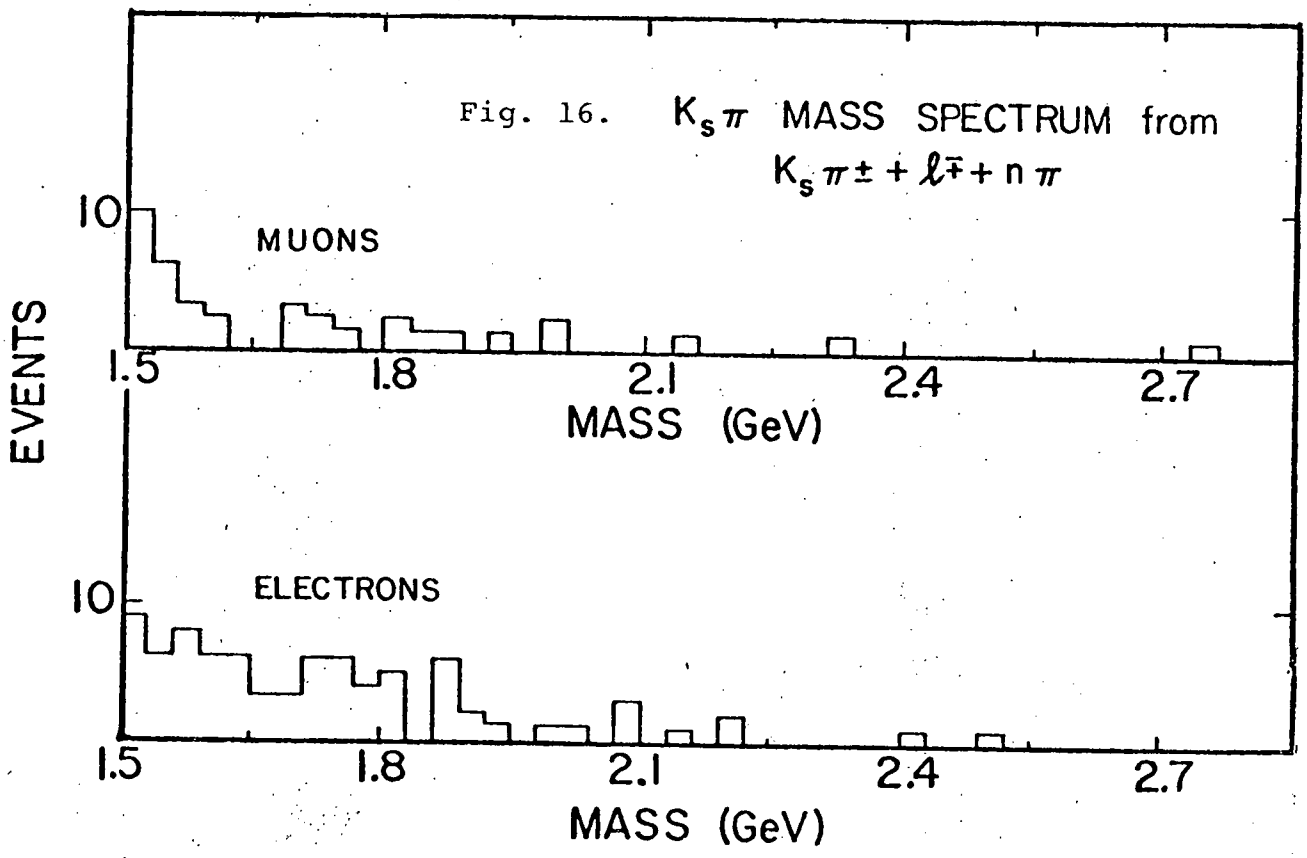

Fig. 16. $K_s\pi$ MASS SPECTRUM from $K_s\pi\pm + \ell\mp + n\pi$

Fig. 17.

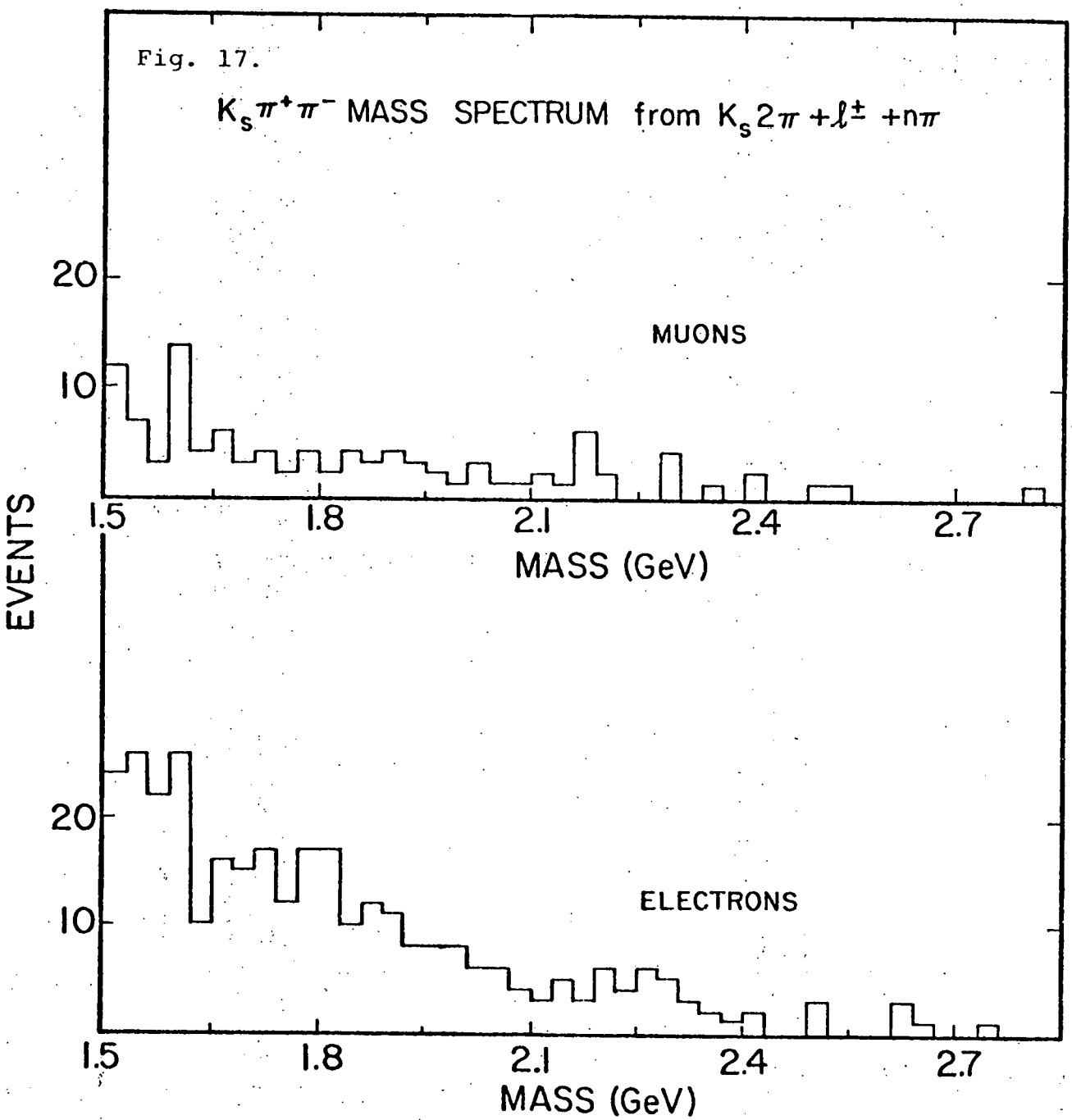
$K_s\pi^+\pi^-$ MASS SPECTRUM from $K_s 2\pi + \ell^\pm + n\pi$
EVENTS
20
10
MUONS
1.5
1.8
2.1
2.4
2.7
MASS (GeV)
20
10
ELECTRONS
1.5
1.8
2.1
2.4
2.7
MASS (GeV)

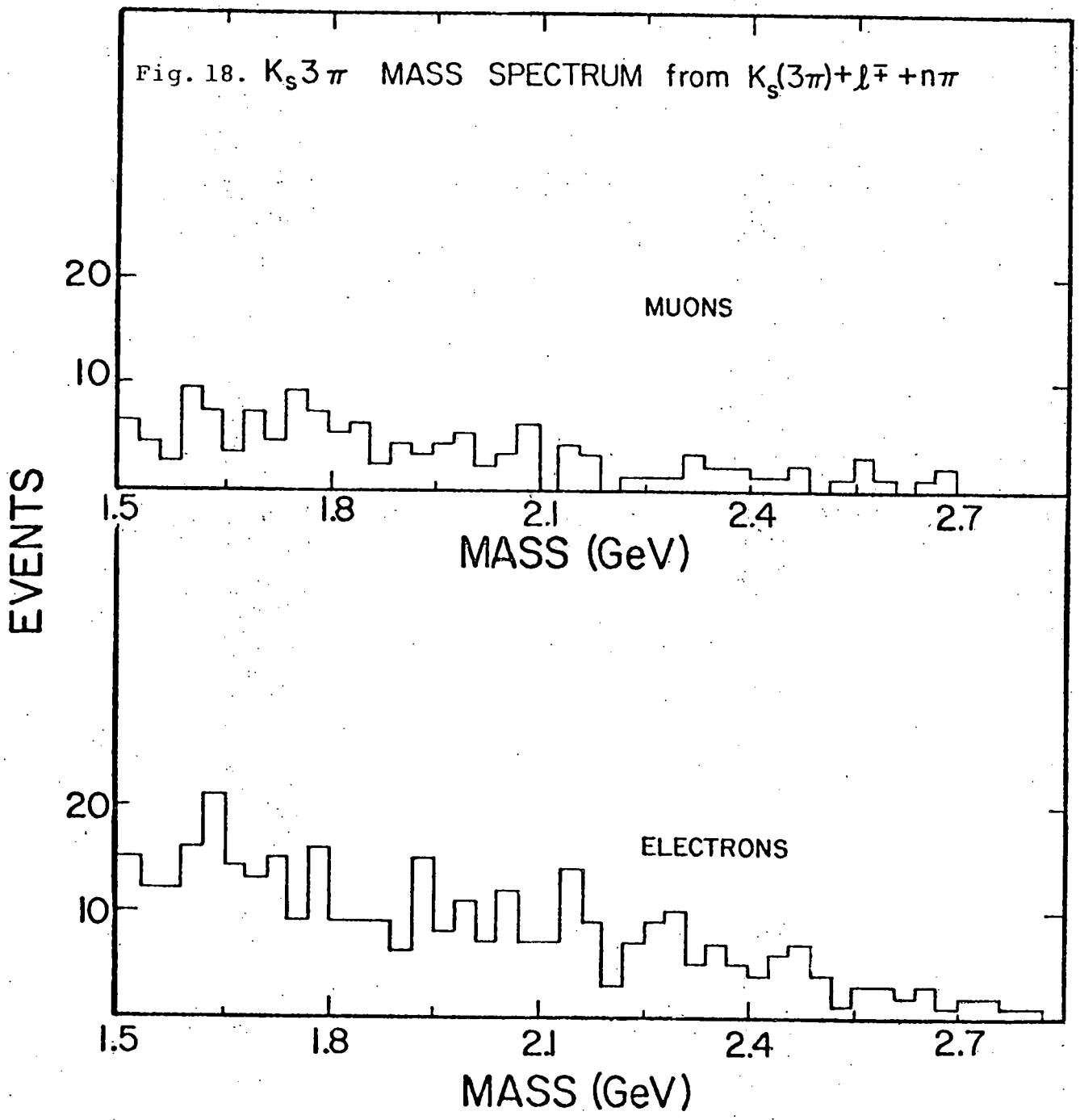

Fig. 18. $K_s 3\pi$ MASS SPECTRUM from $K_s(3\pi)+\ell^{\mp}+n\pi$

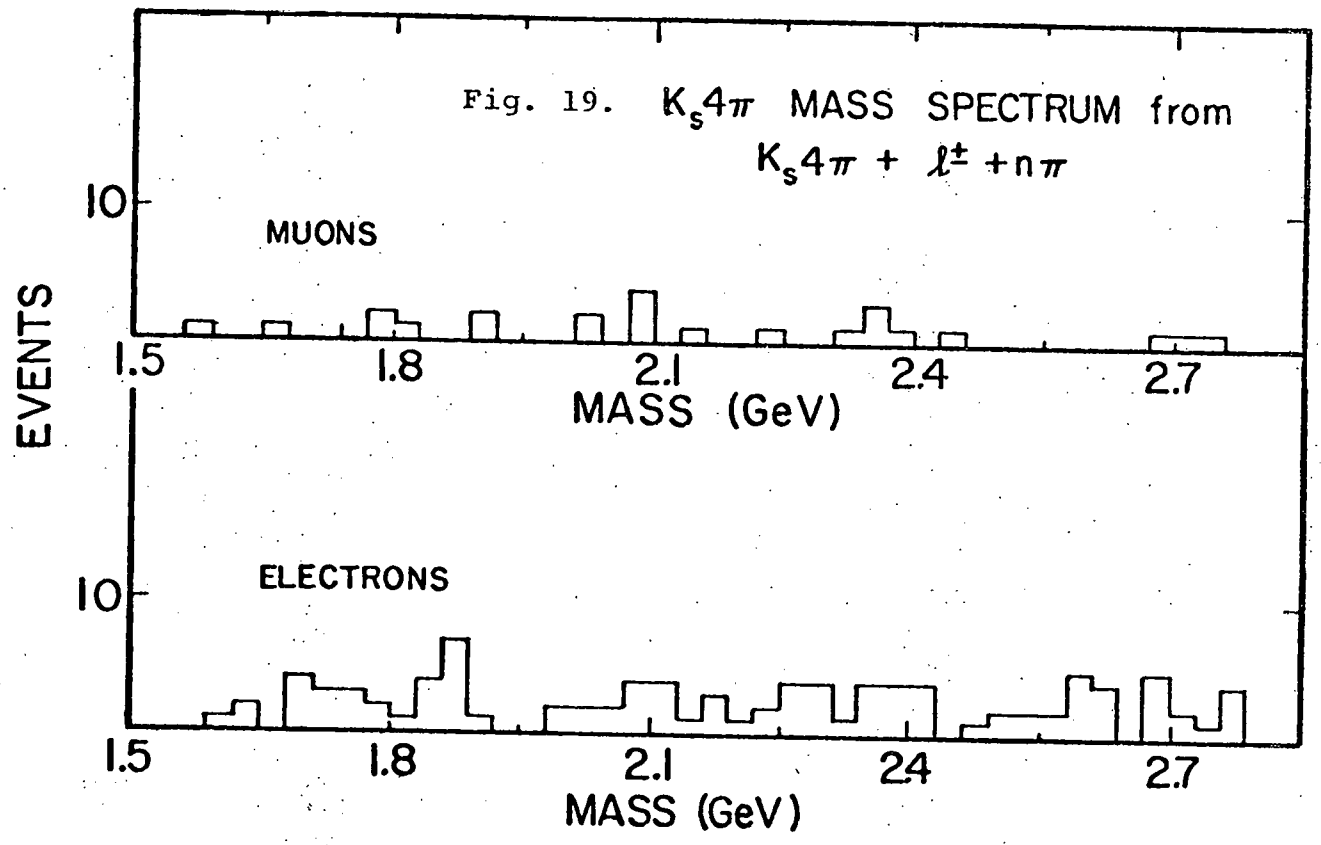

Fig. 19. $K_s 4\pi$ MASS SPECTRUM from $K_s 4\pi + \ell^{\pm} + n\pi$

sample is consistent with the number of background events we expect using the measured π/μ and π/e rejection. If there were enough events with the $K^o_s n\pi^{\pm}$ masses near the D masses we could repeat the background calculation using those events only. Unfortunately the number of events left is small and the statistical errors are large. Within these limitations the number of events observed is consistent with being entirely due to lepton misidentification.

The non-photon induced background is most likely due to neutral hadrons in the beam. For example, a K^o_L will produce $K^o_s n\pi$ events with a cross-section of the order of millibarns whereas the cross-section for photoproduction of K^o_s's is a few microbarns. The ratio of K^o_L's to photons in the beam is of the order of 10^{-2}. Therefore if one selects K^o_s events, the K^o_L background becomes important. To measure this background we insert six radiation lengths of lead into the neutral beam to effectively remove the photons. Background runs were taken interspaced with normal data-taking runs. We find that for the entire mass spectrum approximately 60% of the final lepton-K^o_s events are K^o_L induced.

IV. Sensitivity of Search

In the following section our sensitivity for observing $D\bar{D}$ photoproduction is estimated using the results of the previous section along with theoretical branching ratios and models of the production mechanism. Some experimental information exists on various branching ratios, however one must rely on theoretical models completely for the production mechanism. Therefore the largest uncertainty in obtaining cross sections involves the production model used in the Monte Carlo calculation of the acceptance.

The number of events observed is related to the cross section by

$$N_{evts} = 2\sigma(\gamma + Be \rightarrow D\bar{D} + X)\ B\ \varepsilon\ F\ Acc.$$

where

N_{evts} = Number of events observed

B = Product of branching ratios

$(B(D \rightarrow \ell + \ldots)\ B(D \rightarrow K^{o}n\pi^{\pm})\ B(K^{o} \rightarrow \pi^{+}\pi^{-}))$

ε = Experimental detection efficiency

F = Flux = $N_A\ N_\gamma$

N_A = Effective number of atoms in the target

N_γ = Number of photons in beam

Acc. = Geometric acceptance

A. Flux and Acceptance

The effective number of atoms in the target is given by

$$N_A = \frac{N_o \rho L_{eff}}{A}$$

where

N_o = Avagadro's number

ρ = Density of target material

A = Molecular weight of target material

$$L_{eff} = \int_o^L e^{-\frac{7}{9}\frac{x}{X_o}} dx$$

L = Physical length of target

X_o = Radiation length of target

A 2.46 cm long beryllium target was used for this experiment. Inserting the values for beryllium (ρ = 1.846 gm/cm^3, A = 9 gm, and X_o = 35.7 cm) gives $N_A = 2.96 \times 10^{23}$ cm^{-2}.

The factor N_γ is determined using the photon energy spectrum (Fig. 2) normalized to the quantameter reading for the data sample analyzed. The quantameter measures the photon spectrum power (Qc) in Q coulombs where c is a conversion factor. The quantameter reading for the data sample is $Q = 2.97 \times 10^{-3}$ coulombs which gives

$$Qc = \frac{(2.97 \times 10^{-3} \text{ coulombs})}{(416 \text{ ions/GeV})(1.60 \times 10^{-19} \text{ coulombs/ion})} = 4.46 \times 10^{13} \text{ GeV}.$$

The photon spectrum $(\frac{dN_\gamma}{dK})$ is normalized such that the photon spectrum power ($Qc = \int K \frac{dN_\gamma}{dK} dK$) agrees with Qc measured by the quantameter. For the final states considered the acceptance for events produced from photons of less than 100 GeV is negligible. We therefore calculate N_γ(K = 100-300 GeV), the number of photons with energy between 100 and 300 GeV. The result is N_γ(K = 100-300) = 1.13×10^{11} photons.

The model used for the Monte Carlo calculation of the accep-

tance assumes a $D\bar{D}$ pair is produced with a mass ($M_{D\bar{D}}$) and a transverse momentum according to $e^{-bp_\perp}$. We have assumed the $D\bar{D}$ pair is produced near threshold (hence $M_{D\bar{D}} \simeq 4.0$ GeV) and we have taken $b = 2$. All decays were generated according to isostropic angular distributions in the center of mass. The energy of events was generated with an exponential distribution ($e^{-K/47}$) according to the slope of the measured photon energy spectrum. Each event is required to have all tracks pass through the detector, since the single lepton trigger contained a veto on wide angle tracks missing the detector. The acceptance values obtained for $K^0_S n\pi^\pm$ states accompanied by leptons are .02, .015, .012, and .008 for $n = 1, 2, 3, 4$. The acceptance is reduced by approximately two if $M_{D\bar{D}}$ is taken to be 5.0 GeV rather than 4.0 GeV. The acceptance is relatively insensitive to the value of b, for example, taking $b = 6$ changes the acceptance by less than 20%.

In addition to the dependence on $M_{D\bar{D}}$ and b, the acceptance depends on the number of tracks in the event, because of the veto on wide angle tracks used in the trigger. We have taken $\Gamma(D \to K\ell\nu) = \Gamma(D \to K^*\ell\nu)$ and together to be 80% of all semi-leptonic decays which is consistent with experimental data. Presumably multi-pion decays ($D \to K\pi\pi\ell\nu$, etc.) will make up the remaining 20% and will be suppressed due to our veto on wide angle particles. If all the decays occurred with K*, the acceptance will be reduced by about 30% due to the additional tracks from the K* decays. From the SLAC data we know the dominant source of D^0's is from $D^{*0}\bar{D}^{*0}$ or $D^0\bar{D}^{*0} + D^{*0}\bar{D}^0$ where $D^{*0} \to D^0\pi^0$(or γ). The π^0 (or γ) will not trigger the wide angle veto counters. For $D^\pm$

production, however, one finds either one or no additional charged pions, for example

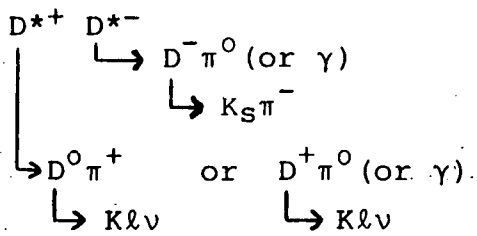

We have assumed $\Gamma(D^{*+} \to D^0\pi^+) \simeq \Gamma(D^{*+} \to D^+\pi^0(\text{or } \gamma))$. Decays with an additional charged pion from the D* decay are suppressed by a factor of about two relative to those with no additional tracks.

B. Experimental Detection Efficiency

The experimental detection efficiency includes the electronic livetime, the efficiency of the lepton cuts, and the detection efficiency of counters and MWPC's. The electronic livetime includes the logic livetime as well as system livetime as discussed in the section on electronics (II.C). The overall electronic livetime is then

$$\varepsilon(\text{livetime}) = \frac{\Sigma \text{ Pin logic} \cdot \bar{D}}{\Sigma \text{ Pin logic}} \times \frac{\Sigma \text{ MG} \cdot \bar{D}}{\Sigma \text{ MG}}$$

where $\bar{D}$ means the appropriate electronics are live and MG means master gate. The result is ε(livetime) = 61% for both the single muon and the single electron pin logics (or triggers).

The efficiency of identifying mouns has been studied in special test runs where the collimators are closed and single upstream muon tracks are used to find the efficiency of the muon cuts. The result is ε(muon cuts) = 96%. For electrons the efficiency is more difficult to determine. For two track events, the efficiency of electron cuts can be studied using electron pair

data taken in special spectrum and calibration runs. The E/p and f cuts are 90% efficient for two track events. In higher multiplicity events some fraction of the electrons will be lost due to one or more tracks hitting in or near the same shower counters. We estimate that on the average roughly two-thirds of the single electrons will be lost to this overlap problem, giving an electron efficiency of approximately 60%. The efficiency of the counters and MWPC requirements used in the master gate and single lepton triggers gives $\varepsilon(\text{counter + MWPC}) \simeq .90$. The details of these estimates are described in References 41 and 43. So finally the overall detection efficiency is given by

$$\varepsilon_{tot} = \varepsilon(\text{livetime})\ \varepsilon(\text{lepton cuts})\ \varepsilon(\text{counter + MWPC}).$$

The results are $\varepsilon_{tot}(\text{muons}) = .53$ and $\varepsilon_{tot}(\text{electrons}) \simeq .30$.

C. Cross Section Estimates

For estimating cross sections we have used muons rather than electrons, because of the better detection efficiency and hadron rejection for muons. The results of the calculations of N_A, N_γ, and $\varepsilon_{tot}(\text{muon})$ of the previous sections can be combined with $B(K^o \to \pi^+\pi^-) = .34$ to give

$$\sigma(\gamma + Be \to D\bar{D} + X)\ B(D \to \ell + \ldots)\ B(D \to K^o n\pi^{\pm}) = \frac{N_{evts}}{Acceptance} \times (.082\ \text{nb}).$$

The masses of the D^o and D^+ mesons obtained at SLAC are 1868 ± 2 MeV and 1876 ± 15 MeV respectively. The mass resolution has been calculated using a Monte Carlo program. This is done by generating horizontal and vertical positions in each chamber with Gaussian distributions about the projected position in that chamber. The calculated mass resolution (full width at half maximum) for

$K^0_S n\pi^\pm$ is about 40, 30, 25, and 20 MeV for n = 1, 2, 3, 4. For the purpose of calculating upper limits, we have taken a mass cut about the D^0 mass that includes one standard deviation ($\pm$ 1σ) on either side of a narrow mass peak. For the D^+ mass cuts, N_{evts} is the maximum number of events in any mass bin (width $\pm$ 1σ) in the region of the D^+ mass. (This is necessary since the uncertainty of the D^+ mass is larger than our mass resolution for $D^\pm \to K^0 3\pi^\pm$.) The number of events observed is then corrected for the ($\pm$ 1σ) cut in mass. The values of $\sigma(\gamma + Be \to D\bar{D} + X)\ B(D \to \ell + \ldots)\ B(D \to K^0 n\pi^\pm)$ obtained are shown in Columns IA and IB of Table II. Column IA shows the maximum cross section obtained by a straightforward calculation attributing all observed events within the D mass cut to D mesons. Column IB shows the 90% confidence level upper limits on the cross sections found by estimating the level of background using events in neighboring mass regions of the D meson ($\pm$ 150 MeV). Increasing the width of the mass cut from two to four standard deviations does not affect the upper limits appreciably.

In order to estimate $\sigma(\gamma p \to D\bar{D} + X)$, we have assumed $B(D \to e + \ldots) = B(D \to \mu + \ldots) = .10$ and $B(D \to \text{hadrons}) = .80$. As discussed in the introduction the statistical isospin model gives predictions for $B(D \to K^0 n\pi^\pm)$ which are consistent with the SLAC results with the exception of $B(D^\pm \to K^0\pi^\pm)$. We have used $B(D^\pm \to K^0\pi^\pm) = .03$ implied by the experimental data rather than $B(D^\pm \to K^0\pi^\pm) = .10$ predicted by the model. To convert the cross section on a beryllium nucleus to the cross section per nucleon we have divided by nine. The resulting cross section estimates

Table II: Hadronic Events in Coincidence with Muons

Column IA, IIA: $N_{evts} = N \equiv$ Background events observed within D mass cut

Column IB, IIB: $N_{evts} = N' \equiv$ 90% confidence level upper limits on excess events based on estimated background level within D mass cut

Hadronic Type Accompanying Muon	Acceptance	N	N'	σ_{Be} x B(D → ℓ + ...)x B(D → $K^o n\pi^{\pm}$) Column I (nanobarns) A	Column I (nanobarns) B	Column II* (nanobarns) $\sigma(\gamma p \to D\bar{D} + X)$ A	Column II* (nanobarns) B
$K^o\pi^{\pm}$	.02	1	2.9	6.2	18	230	660
$K^o\pi^+\pi^-$	.015	4	3.5	32	28	360	310
$K^o\pi^{\pm}\pi^+\pi^-$	.012	3	3.8	30	38	370	470
$K^o 4\pi$	.008	1	2.5	15	37	540	1370

*Assumed Branching Ratios:

Semi-leptonic μ = 0.10

$K^o\pi$ = .03

$K^o 2\pi$ = .10

$K^o 3\pi$ = .09

$K^o 4\pi$ = .03

for $D^{\pm}$ and $D^0(\bar{D}^0)$ production per nucleon are given in Column II of Table II. The predictions for $\sigma(\gamma p \rightarrow D\bar{D} + X)$ range from 50 to 500 nb as discussed in the introduction.

In conclusion, we have searched for the photoproduction of a pair of charmed mesons ($D\bar{D}$) followed by the semileptonic decay of one D meson and the hadronic decay into $K^0_S n\pi^{\pm}$ of the other D meson. We observe no statistically significant accumulation of events at the D meson masses in the $K^0_S n\pi^{\pm}$ mass spectrum. Establishing firm upper limits is difficult because of uncertainties in the production mechanism and branching ratios. The estimates of this experiment's level of sensitivity are comparable to the upper range of predictions of $\sigma(\gamma p \rightarrow D\bar{D} + X)$ of about 500 nb.

Appendix A

Photon Spectrum and Shower Detector Calibrations

The photon energy spectrum and the shower detector calibration constants were measured using electron pair data. The measured photon spectrum is used in cross section calculations (see section IV.A). The calibration constants are used to convert pulse height information from the shower detector into energy.

The electron pairs are produced in special spectrum and calibration runs in which a 0.04 radiation length lead foil is placed in front of the horizontal bending magnet (M1 in Fig. 11). The purpose of the horizontal bending magnet is to spread electron tracks over the shower detector. The trigger used for this data was MG · (MWPC >1) where the master gate (MG) was B3 · (L + R) >0 (see Table I on page 14 for abbreviations).

The data used to determine the calibration constants was required to pass the following cuts:

1. Two tracks of opposite charge
2. ≤ 2 mr opening angle
3. The tracks within 5 cm of active area of the shower detector array
4. The tracks must pass through one and only one front counter and one and only one back counter (within 3.8 cm of the top or bottom of each counter)

In this way tracks were selected which deposited all their energy in a single front counter and a single back counter. The energy measured in the shower detector (E) is then given by

$$E = \alpha_F N_F + \alpha_B N_B$$

where α_F (α_B) is the calibration constant for the front (back) shower counter and N_F (N_B) is the pulse height (ADC) reading for the front (back) counter. Electrons should deposit all their energy in these two counters, so we have E/p = 1, where E is the energy measured by the shower detector and p is the momentum measured by the spectrometer. The calibration constants (α_F, α_B) are obtained by minimizing the energy resolution subject to the constraint that E/p should have an average value of one. In this way the calibration constants for each of the forty-six counters in the shower detector were found. Details of this method and also of the light pulser system used to monitor the stability of the shower counters are included in Reference 43. The E/p distribution for electrons and pions is shown in Fig. 14. The energy resolution is given by

$$\frac{\Delta E}{E}(\%) \simeq \frac{40}{\sqrt{E}} + 2.5.$$

The same electron data was also used to determine the photon spectrum. Events used for the photon spectrum were required to pass the following cuts:

1. Two tracks of opposite charge
2. $\lesssim$ 2 mr opening angle

The photon spectrum is obtained by correcting the raw data for geometric acceptance and electronic livetime. The geometric acceptance is calculated as a function of the photon energy and the fraction of this energy taken by the positron. The quantameter readings were used to normalize electron data collected at

several magnet currents which were required to scan the full photon energy range. The resulting photon spectrum is shown in Fig. 2.

Appendix B

Semileptonic Decays of Charmed Baryons

As discussed in the introduction, our experiment has observed a narrow resonance which is a candidate for the charmed antibaryon ($\bar{\Lambda}_c$) decaying into $\bar{\Lambda}3\pi^-$.[16] The observation of leptons in coincidence with the $\bar{\Lambda}3\pi^-$ signal would support the $\bar{\Lambda}_c$ interpretation, since charmed baryons are expected to be photoproduced in pairs ($\Lambda_c\ \bar{\Lambda}_c$) and could have significant semileptonic decay modes such as $\Lambda_c \to \Lambda\ell^+\nu$. The $\Lambda 3\pi^+$ decay of the charmed baryon (Λ_c) was not observed, possibly because the background is larger for Λ events than for $\bar{\Lambda}$ events. This is due to the excess of baryons over antibaryons in the neutral beam and the production target. If a substantial fraction of charmed baryons do decay semileptonically, then one might hope to reduce the background enough to observe the decay $\Lambda_c \to \Lambda 3\pi^+$ by requiring leptons.

An analysis of events containing lepton-Λ (or $\bar{\Lambda}$) candidates similar to the lepton-K_S^0 analysis (Section III) has been done. The differences are that the data sample includes a variety of triggers (multi-hadron, single lepton, and dilepton) and a Λ(or $\bar{\Lambda}$) is selected rather than a K_S^0. A neutral V^0 which is not identified as a K_S^0 and has an invariant mass of 1116 ± 2 MeV assuming the more energetic particle to be a proton (anti-proton) is identified as a Λ ($\bar{\Lambda}$).

Using this data sample we have searched for the reaction

$$\gamma + \mathrm{Be} \to \Lambda_c\ \bar{\Lambda}_c \begin{cases} \hookrightarrow \bar{\Lambda}\pi^- \text{ or } \bar{\Lambda}3\pi^- \\ \hookrightarrow \ell^+ + \ldots \end{cases}$$

or the charge conjugate final state containing Λ's. The mass spectrum obtained for $\Lambda\pi^+$, $\Lambda 3\pi^+$, $\bar{\Lambda}\pi^-$, and $\bar{\Lambda}3\pi^-$ occurring in coincidence with opposite charge leptons has been studied. The $\bar{\Lambda}3\pi^-$ and $\Lambda 3\pi^+$ mass spectrum are shown in Fig. 20. We observe no statistically significant enhancements near the Λ_c or $\bar{\Lambda}_c$ mass. There are 106 $\bar{\Lambda}3\pi^-$ events with extra tracks in a 75 MeV mass bin at the $\bar{\Lambda}_c$ mass. The background in each adjacent 75 MeV bin above and below the $\bar{\Lambda}_c$ peak contains about sixty events. Based on the reduction of all $\bar{\Lambda}3\pi^-$ masses outside the $\bar{\Lambda}_c$ peak, we expect a background of about 4.5 muons and 3.6 electrons from events within the $\bar{\Lambda}_c$ mass peak. We observe seven muon candidates and five electron candidates within the $\bar{\Lambda}_c$ mass peak. Thus there is no statistically significant evidence in our data sample for an appreciable branching ratio to semileptonic decay modes of charmed baryons.

Fig. 20. $\bar{\Lambda}(3\pi)^-$ MASS SPECTRUM from $\Lambda(3\pi)^- + \ell^+ + n\pi$

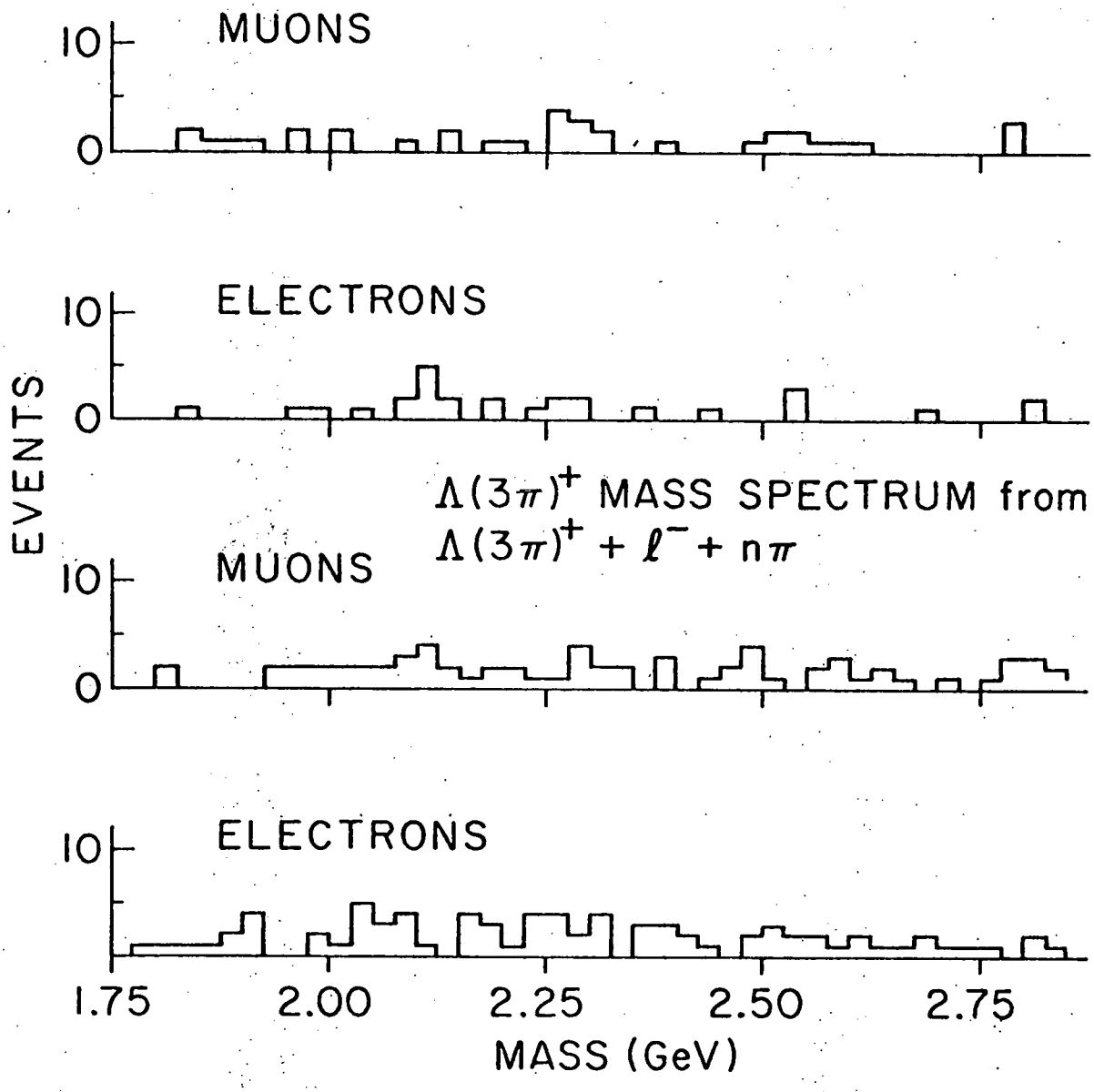

List of References

1. J. D. Bjorken and S. L. Glashow, Phys. Lett. 11, 255 (1964).
2. S. L. Glashow, et al., Phys. Rev. D2, 1285 (1970).
3. M. K. Gaillard, et al., Rev. Mod. Phys. 47, 277 (1975).
4. J. J. Aubert, et al., Phys. Rev. Lett. 33, 1404 (1974).
5. J. E. Augustin, et al., Phys. Rev. Lett. 33, 1406 (1974).
6. V. Luth in Xth International School for High Energy Physics, Baku, USSR (1976).

   B. H. Wiik and G. Wolf in Les Houches Summer School (1976).
7. G. S. Abrams, et al., Phys. Rev. Lett. 33, 1453 (1974).
8. S. Okubo, Phys. Lett. 5, 165 (1963); G. Zweig, unpublished; Suppl. to Prog. Theor. Phys. 37-38, 21 (1966).
9. G. Flugge, reported at Washington APS Meeting, April 1977.
10. M. S. Chanowitz and F. J. Gilman, SLAC preprint PUB-1746(1976).
11. F. J. Gilman in Particles and Fields Conference at Brookhaven (1976).
12. A. Salam in Proceedings of the 8th Nobel Symposium (1968).

    S. Weinberg, Phys. Rev. Lett. 19, 1264 (1967).
13. A. De Rújula, et al., Phys. Rev. D12, 147 (1975).
14. G. Goldhaber, et al., Phys. Rev. Lett. 37, 255 (1976).
15. I. Peruzzi, et al., Phys. Rev. Lett. 37, 569 (1976).
16. B. Knapp, et al., Phys. Rev. Lett. 37, 882 (1976).
17. R. Schwitters in Particles and Fields Conference at Brookhaven (1976).
18. B. Knapp in Particles and Fields Conference at Brookhaven (1976). (The effect is about 2.5 standard deviations above background.)
19. A. De Rújula, et al., Phys. Rev. Lett. 37, 398 (1976).
20. K. Lane and E. Eichten, Phys. Rev. Lett. 37, 477 (1976).
21. G. Goldhaber reported at Chicago APS Meeting, March 1977.

22. G. J. Feldman, SLAC-PUB-1919 (1977).

23. B. Humpert, SLAC-PUB-1829 (1976).

24. DASP-Collaboration, W. Braunschweig, et al., Phys. Lett. 63B, 471 (1976).

25. J. Burmester, et al., DESY Report 76/53 (1976).

26. G. J. Feldman, et al., Phys. Rev. Lett. 38, 117 (1977).

27. J. von Krogh, et al., Phys. Rev. Lett. 36, 710 (1976).

H. Deden, et al., Phys. Lett. 58B, 361 (1975).

J. Blietschau, et al., Phys. Lett. 60B, 207 (1976).

28. A. Benvenuti, et al., Phys. Rev. Lett. 34, 419 (1975).

A. Benvenuti, et al., Phys. Rev. Lett. 35, 1199, 1203, 1249 (1975).

B. C. Barish, et al., Phys. Rev. Lett. 36, 939 (1976).

29. E. G. Cazzoli, et al., Phys. Rev. Lett. 34, 1125 (1976).

30. J. Sarracino, Ph.D. Thesis, University of Illinois (1976).

31. D. M. Ritson, Preprint SLAC-PUB-1728 (1976).

32. D. Sivers, et al., Phys. Rev. D13, 1234 (1976).

33. M. Chen, et. al., Preprint UM, HE 76-17 (1976).

34. V. Barger, et al., Preprint COO-564 (1977).

35. I. Hinchliffe and C. H. Llewellyn Smith, Nuclear Physics B114, 45 (1976).

36. R. P. Nabavi, et al., IPNO/TH 77.08 (1977).

37. M. Peshkin and J. Rosner, preprint COO 2220-93 (1976).

38. J. Rosner at Orbis Scientiae, Coral Gables, Florida (1977).

39. F. Gilman at Orbis Scientiae, Coral Gables, Florida (1977).

40. D. Hitlin, preprint SLAC-PUB-1869 (1977).

41. D. Nease, Ph.D. Thesis, Cornell University (1975).

42. D. Wheeler, Ph.D. Thesis, University of Illinois (1975).

43. L. Cormell, Ph.D. Thesis, University of Illinois (1975).

44. T. Wijangco, Ph.D. Thesis, Columbia University (1976).

45. F. Harris and D. Yount, Nucl. Inst. and Meth. 114, 357 (1974).

Vita

Richard Neal Coleman

received a Bachelor of Science degree in Physics from the University of California, Berkeley, in 1972 and a Master of Science degree from the University of Illinois in 1974. Since 1974 he has held teaching and research assistantships in the Physics Department of the University of Illinois.